https://doi.org/10.5194/egusphere-2025-6540
Preprint. Discussion started: 12 January 2026

Ballistic projectile hazard of major explosions and paroxysms at Stromboli (Italy) with uncertainty quantification: 2. Conditional and temporal probability maps

Andrea Bevilacqua[(1)], Augusto Neri[(1)], Patrizia Landi[(1)], Paola Del Carlo[(1)], Massimo Pompilio[(1)], Peter Baxter[(2)]

[1] Istituto Nazionale di Geofisica e Vulcanologia, Sezione di Pisa, Pisa, 56125, Italy
[2] Department of Public Health and Primary Care, University of Cambridge, Cambridge, CB2 0SR, United Kingdom.

Correspondence to: Augusto Neri (augusto.neri@ingv.it)

Abstract. This study presents the first probability hazard maps of the areas potentially affected by ballistic fallout from major explosions and paroxysms at Stromboli, based on mathematical analyses of the extensive historical and recent records of its explosive activity. This novel approach develops and integrates three statistical models that describe ballistic fallout patterns under different assumptions and considering the associated uncertainty. Model 1 mirrors the areas observed to be affected in the past, whereas Models 2 and 3 address data under-sampling and morphological/dynamics changes assuming independency between ballistic distance and dispersal direction. By combining these models, robust and conservative ballistic fallout hazard maps are produced for major explosions and paroxysms, and for the two categories combined together by assuming a relative proportion. The new combined maps highlight the most exposed areas of the island and quantify the probability of being affected in the case of a major explosion or paroxysm. For instance, the NE trails at 600 m would have ≈25% probability of ballistic fallout, while the Labronzo trail ≈8% and 5% probability at 400 and 290 m, respectively; the entire village of Ginostra would be affected with ≈3% probability. Combining such maps with a temporal model of occurrence of the events, first probability maps of ballistic fallout in the next 10 and 50 years are presented. Results are moderately influenced by mapping uncertainties and by the assumed proportion between major explosions and paroxysms. These findings open the way to individual and societal risk assessments for this phenomenon at Stromboli.

Short summary. Using historical records and mathematical models, researchers created maps that show the probability of different areas being affected by ballistic fallout from volcanic eruptions in Stromboli, Italy. Hazard maps were developed for both major explosions and paroxysms, as well as for the two categories combined together by assuming a relative proportion. By using a temporal model of the explosive events, first probability maps of ballistic fallout in the next 10 and 50 years are finally presented.

https://doi.org/10.5194/egusphere-2025-6540
Preprint. Discussion started: 12 January 2026

1 Introduction

Ballistic projectiles are one of the main hazards associated with explosive volcanic activity (Wilson, 1972). In fact, ballistics are the leading cause of deadly incidents within a 5 km range of active volcanoes worldwide, particularly those popular with tourists, such as Galeras (Colombia), Popocatepetl (Mexico), Yasur (Vanuatu), Tongariro (New Zealand), Ontake and Shinmoedake (Japan) (Maeno et al., 2013; Brown et al., 2017; Fitzgerald et al., 2018). In addition, ballistic projectiles can damage buildings and infrastructures (Biass et al., 2016; Williams et al., 2017; Massaro et al., 2022), and ignite fires (Turchi et al., 2020; Guardo et al., 2024; Iacono et al., 2025).

Stromboli (Italy) is a 3 × 4 km volcanic island strongly affected by ballistic hazard (Barberi et al., 1993; Rosi et al., 2013). The volcano reaches a height of 924 m above sea level and is characterized by a distinctive horseshoe-shaped depression known as Sciara del Fuoco in the NW section of the volcano, and another smaller depression to the SE, called Rina Grande (Fig. 1). For many centuries, at least since the Middle Ages (e.g., Re et al., 2025), the volcano has shown almost continuous explosive activity centered in several craters within a relatively leveled area, called Crater Terrace and situated at approximately 750 m elevation atop Sciara del Fuoco, as depicted in Figure 1. Hazardous ballistics are mostly generated during major explosions and paroxysms that interrupt the persistent mild Strombolian activity of the volcano (Barberi et al., 1993; Bertagnini et al., 2011; Rosi et al., 2013; Bevilacqua et al., 2020a).

The hazardous area affected by large ballistic projectiles is typically considered the main distinguishing factor for differentiating between ordinary activity, major explosions, and paroxysms (Barberi et al., 1993; Pompilio et al., 2010; Rosi et al., 2013; Bevilacqua et al., 2020a). This area is confined to the Crater Terrace and the upper Sciara del Fuoco during ordinary activity, extends to the summit area of the volcano and the Sciara del Fuoco during major explosions, and can reach down to lower elevations across much of the island, sometimes even extending beyond the shoreline, during paroxysms.

This phenomenon represents a direct peril not only for the hundreds of tourists climbing the volcano for short periods of time, but also for the volcanological guides and the scientists who are exposed to this hazard much longer, and the small communities living along the island coast that live full-time on the volcano.

Ballistic hazard has been mostly described by using two different approaches: 1) data analyses relying on field work and past observations such as the distribution of ballistics ejected in previous explosions (Bertagnini et al., 1999; 2008; Coltelli et al., 2000; Rosi et al., 2006; Andronico and Pistolesi, 2010; Pistolesi et al., 2011; Giordano and De Astis, 2021; Andronico et al., 2021); 2) numerical simulation of ballistic trajectories thus relying on the complex reconstruction of the explosion dynamics and the associated source conditions (Fitzgerald et al., 2014; Alatorre-Ibargüengoitia et al., 2016; Bertin, 2017; Bernard, 2018).

In the former approach, a limited dataset on the ballistic distribution would produce poor results with very large uncertainty. In fact, impulsive volcanic explosions that eject ballistic bombs (as those occurring at Stromboli) are usually made of multiple oriented blasts and different events usually affect significantly different areas. Moreover, the lack of data in the less

https://doi.org/10.5194/egusphere-2025-6540
Preprint. Discussion started: 12 January 2026

accessible sectors of the volcano (such as Sciara del Fuoco at Stromboli) could be significant. Vice versa, in the latter approach based on numerical models, the complex dynamics of the gas-particle interactions occurring in the explosion can have a major effect on the reconstruction of the input conditions and therefore on the trajectories of the ejecta (de'Michieli Vitturi et al., 2010; Kostantinou, 2015; Taddeucci et al., 2017; Rosi et al., 2018; Massaro et al., 2022). Moreover, in both approaches, the structures of the jet and the direction of the ballistics can be strongly affected by the ever-changing morphology of the active craters and shallow conduits, and by the variable explosive dynamics (Ogden et al., 2008; Esposti Ongaro et al., 2008; Vanderkluysen et al., 2012; Valentine et al., 2012; Carcano et al., 2013; Taddeucci et al., 2013; Tsunematsu et al., 2015; Graettinger et al., 2015). Neither one of these two approaches has ever been thoroughly applied to Stromboli in the construction of quantitative probabilistic hazard maps.

In this work, we aim at developing probabilistic hazard maps of this phenomenon at Stromboli based on the large amount of information describing the past explosive activity of the volcano and also considering the effect of some main sources of uncertainty. This input information is described in detail in a companion study (Bevilacqua et al., submitted) and briefly summarized in the following sections.

We rely on data analysis of the distance, direction and area affected by ballistic particles of a considerable number of major explosions (43 events) and paroxysms (24 events) occurred at Stromboli, in order to define first probability hazard maps of ballistic dispersal. In particular, the models we developed are doubly stochastic in the sense that they allow to carefully quantify the effects of the uncertain reconstruction of past ballistic projectiles distributions (Sparks & Aspinall, 2004; Marzocchi & Bebbington, 2012; Bevilacqua et al., 2015). In fact, the maps are represented using ill-constrained information, treated as a random array, and we separately estimate this epistemic uncertainty from the aleatoric probability model of future phenomena (Bebbington, 2013; Bevilacqua et al., 2016; 2018).

In section 2 we briefly describe the input data and information from the companion study (Bevilacqua et al., submitted). In section 3 we describe the approach and models adopted to produce the hazard maps by Monte Carlo simulation, and to statistically combine the maps associated with major explosions and paroxysms. In section 4 we present the ballistics probability maps of the two distinct categories of major explosions and paroxysms, the combined map of the two categories (major explosions plus paroxysms), as well as the probability curves at various distances from the craters and elevations above sea level for the most relevant cases investigated. Finally, in section 5 we present examples of ballistic hazard assessments incorporating the hourly probability estimates of major explosions and paroxysms at Stromboli as computed by a temporal model of occurrence of these phenomena.

https://doi.org/10.5194/egusphere-2025-6540
Preprint. Discussion started: 12 January 2026

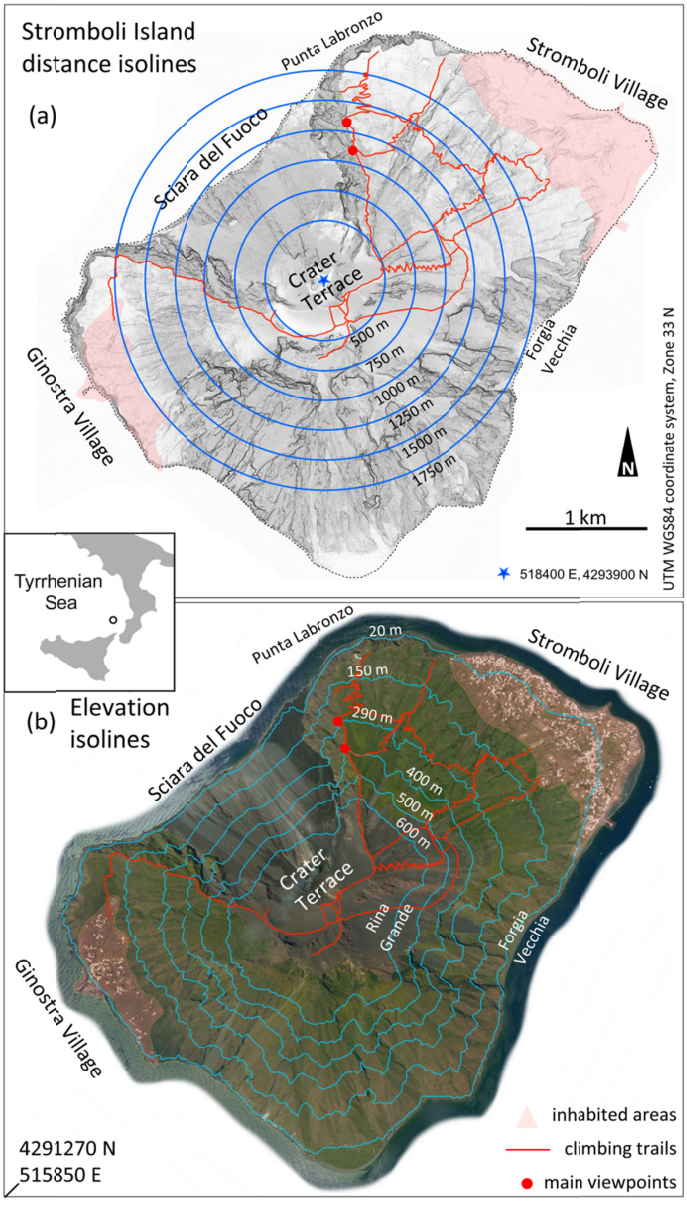

Figure 1: Overview of the island of Stromboli. (a) shows a vertical shaded relief and distance isolines from 500 m to 1750 m with respect to the center of the Crater Terrace (blue star). (b) shows a satellite/aerial photo orthomosaic and a selection of elevation isolines. Red dots mark the main viewpoints accessed by tourists and volcanological guides, climbing trails are reported in red, and inhabited areas are shaded in pink.

https://doi.org/10.5194/egusphere-2025-6540
Preprint. Discussion started: 12 January 2026

2 Data

To construct the hazard maps illustrated in the Results section, we relied on the mapping method and data analysis described in companion study Bevilacqua et al., (submitted). The main assumptions and limitations of this study were: (i) we used all available ground and remote observations of past events, without any assumption on the conditions of the explosive mixture at the source or relying on descriptive models of projectile dynamics; (ii) the focus was on the description of the lithic and scoria clasts larger than 5-10 cm in diameter, a range related to the uncertainty affecting observations, while smaller clasts and pumice fallout were not considered due to their lower impact energies; (iii) the areal density of the projectiles on the ground, which can vary by up to 2 orders of magnitude mostly based on distance from the crater, was not considered in the analysis (Gurioli et al., 2013; Breard et al., 2014; Bisson et al., 2023; Bevilacqua et al., 2024a); as a consequence, our hazard maps refer to the probability to be in an area affected by ballistic fallout if a major explosion or a paroxysm occur.

Based on such assumptions, schematic maps of ballistic projectile fallout were constructed as described in Bevilacqua et al., (submitted). In each simplified map, a proximal axisymmetric part was defined, in addition to 1 to 3 circular sectors, with greater distance ranges, describing the fallout areas. Supporting Figure S1 reports a selection of twelve maps, six major explosions and six paroxysms, exemplifying different distances and directions reached by ballistic projectiles, and showing estimates of distances, directions, and of their uncertainties. In particular, the i-th circular sector of the j-th explosion is fully described by the radial distance D_{ij}, the azimuth angle of the bisector α_{ij}, and the width angle W_{ij}. In this representation, the width of the axisymmetric part is defined as the complementary to 360° of the union of the (1 to 3) directional sectors. Supporting Figure S2 shows the distributions of the distances and of the directions and widths of all the circular sectors of the major explosions and the paroxysms data. See Bevilacqua et al. (submitted) for more details on these circular sectors and their uncertainties.

Figure 2 summarizes the main data analysis outcomes for both major explosions and paroxysms: the exceedance probability functions of the ballistic distances in all directions (including and not the axisymmetric part) (Figure 2a,b); the ballistic direction probability percentage based on estimates from all directional circular sectors (Figure 2c,d); the histograms of the widths of all directional circular sectors (Figure 2e,f). It should be noted that these analyses are conditional on the occurrence of the related type of phenomenon, i.e., major explosions or paroxysms.

As regards the ballistic distances, Figure 2a shows, for the major explosions, a probability of 25% ±2.0% to meet or exceed 500 m, of 6.0% ±1.0% to meet or exceed 750 m, and of 2.5% ±0.5% to meet or exceed 1000 m. Figure 2b, for the paroxysms, shows a probability of 31% ±2.5% to meet or exceed 1000 m, of 16.5% ±4.0% to meet or exceed 1500 m, and of 4.5% ±1.0% to meet or exceed 2000 m, 0.5% ±0.2% to meet or exceed 2500 m. In both cases, by excluding the proximal

https://doi.org/10.5194/egusphere-2025-6540
Preprint. Discussion started: 12 January 2026

axisymmetric part we obtain probabilities to reach a given distance up to 3 times higher with respect to the case with the axisymmetric part included.

As regards the ballistic direction, in Figure 2c, the probability function of the ballistics directions for major explosions has a maximum of 77% ±2% at 140°E ±10°°, i.e., in the SE direction, and a minimum of 0% at 250°E ±10°, i.e., in the SW direction. In Figure 2d, for the paroxysms, the probability function has a maximum of 70% ±9% at 355°E ±10°, i.e., in the N direction, and a minimum of 19% ±2% at 175°E ±10°, i.e., in the S direction. A plateau above 50% is also observed from NE to W clockwise.

Then, as regards the sector width, i.e. the spread of the azimuth angle being impacted, Figure 2e shows that, for major explosions, the mean width value is 90°, with 5th percentile of 41° and 95th percentile of 136°, while, in Figure 2f, for the paroxysms, the mean width value is again 90°, with 5th percentile of 33° and 95th percentile of 183°. However, the total areas affected by paroxysms are 4 to 6 times larger than those of major explosions although the distribution of the areas affected is continuous between the two categories (more details in the companion paper Bevilacqua et al., submitted). All these categorical data are tabulated in the Supporting Material of Bevilacqua et al., (submitted).

The three parameters of distance, azimuthal direction, and width of the described circular sectors determine our simplified representation of the areas affected by ballistic projectiles. However, these tree parameters are not fully described through their 1D distributions, and in Figure 3 we plotted their bivariate plots, which highlight some distinctive patterns. In particular, Figure 3a shows that the greatest distances of major explosions are observed between N and ESE, and Figure 3b shows that those of the paroxysms are clustered in two groups oriented to the NNE and WSW. In addition, Figures 3c and 3d indicate that, as expected at constant explosion energy, the greatest distances tend to correspond to lower widths, especially for the paroxysms. Finally in Figure 3e and 3f the lower widths are clustered towards ESE for the major explosions, NNE and WSW for the paroxysms, confirming their correlation with the greater distances.

It should be noted that major explosions and paroxysms significantly differ in terms of their predominant directions of ballistic dispersal. A possible reason is that the most frequented trails and inhabited areas are the easiest places to survey in the hours/days after the explosions, and their directions roughly include those of peak probability of major explosions and paroxysms, respectively (see Fig. 1). Nevertheless, physical reasons for these asymmetries are also possible, because the paroxysms involve deeper parts of the conduits and are able to re-shape the craters more greatly and deeply than major explosions, as discussed in the companion study Bevilacqua et al. (submitted). For this reason, in the production of robust and conservative hazard maps it was very important to develop *ad hoc* methods to mitigate potential recording biases, as described in this study.

https://doi.org/10.5194/egusphere-2025-6540
Preprint. Discussion started: 12 January 2026

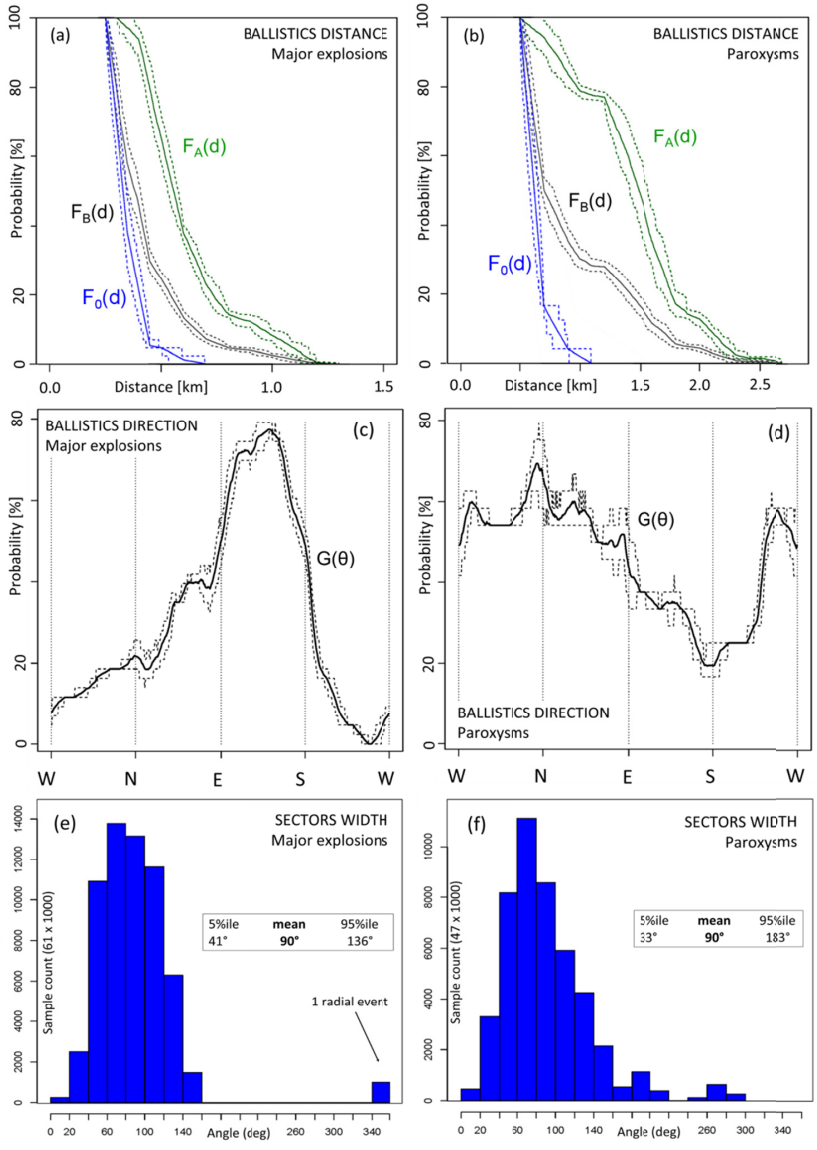

Figure 2: Summary of the data analysis from Bevilacqua et al. (submitted). (a,b) exceedance probability functions of the ballistic distances in all directions (including, F_A, and not including, F_B, the axisymmetric part F_0); (c,d) ballistic direction probability percentage based on estimates from all circular sectors; (e,f) histograms of the widths of all circular sectors. (a,c,e) are related to major explosions, and (b,d,f) to paroxysms. Dashed lines in (a,b,c,d) highlight uncertainty intervals between 5th and 95th percentile values due to the uncertainty in the mapping of ballistic dispersal areas.

https://doi.org/10.5194/egusphere-2025-6540
Preprint. Discussion started: 12 January 2026

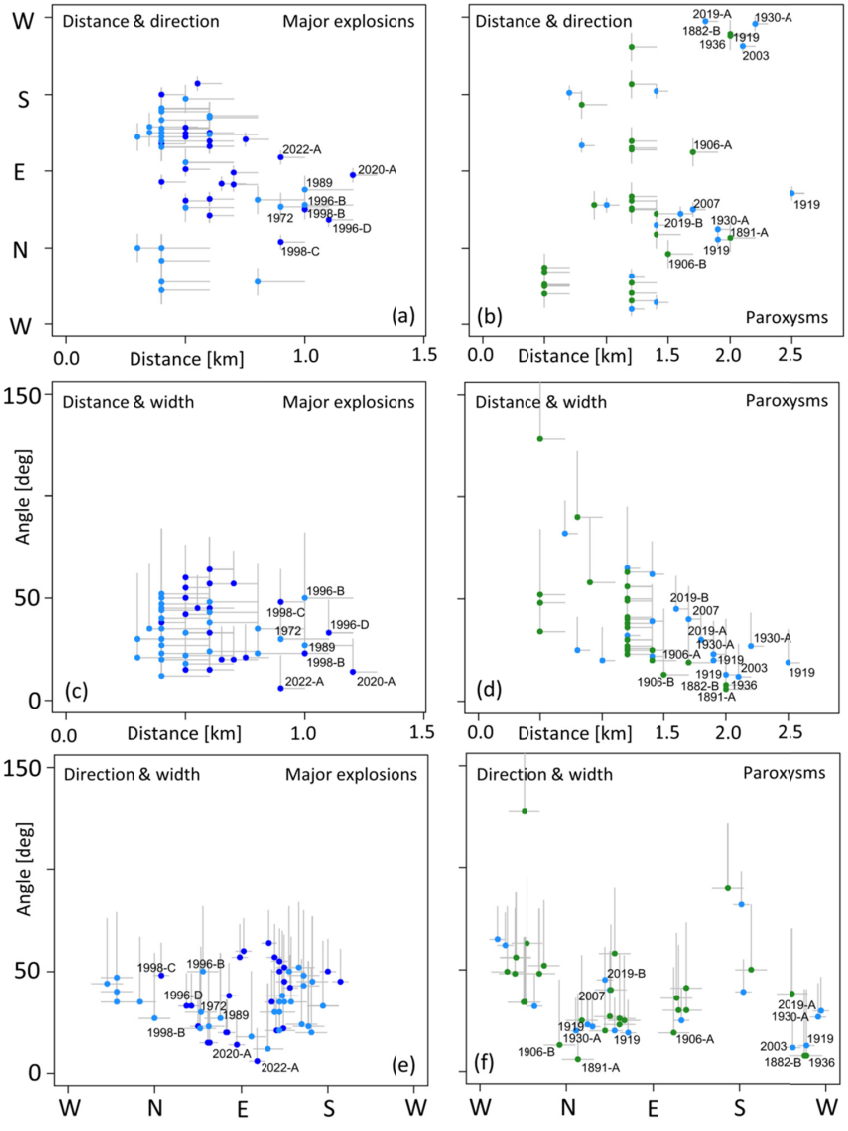

Figure 3: Bivariate plots of the distance, direction, and width of the circular sectors affected by ballistic fallout in the considered major explosions and paroxysms. The grey lines highlight the uncertainty considered, while the colored dots indicate the recorded values. The 8 greater distances recorded for the major explosions and the 14 for the paroxysms are also labeled. Different hues indicate different uncertainty classes (blue: low, azure: intermediate, green: high; see Bevilacqua et al. (submitted) for more details.

https://doi.org/10.5194/egusphere-2025-6540
Preprint. Discussion started: 12 January 2026

3 Methods

3.1 Monte Carlo simulation of the areas affected by ballistic projectiles

Three complementary models were developed to produce the probabilistic ballistic hazard maps presented in the Results section. These models differ in the way they statistically combine the distributions of directions and distances of ballistic projectiles. The spatial domain was parameterized in polar coordinates (d, θ) in $[0, +\infty) \times [0, 360°]$, i.e., the distance and the direction with respect to a center located at 518400 E, 4293900 N, UTM WGS84, Zone 33N, that is approximately the center of the Crater Terrace. Every model provides a spatial function $H^{(k)}(d, \theta)$, with k=1,2,3, that estimates the probability to be in an area affected by ballistic fallout. All these estimates are conditional on the occurrence of a major explosion or paroxysm and are time-homogeneous in the way they account for past events data.

The first model, called Model 1, is the most obvious and directly utilizes the spatial frequency of past events, accounting for the observed dependency between distance and direction. Specifically, at each point (d, θ) in the map, we estimate the percentage of explosions that affected that point. That is:

$$H^{(1)}(d, \theta) = |\{j : (d, \theta) \in S_j\}|/N, \quad (1)$$

where S_j is the total area affected by the ballistic projectiles of the j-th explosion, and N is the total number of the explosions in the dataset. This approach assumes that distance and direction of ballistic projectiles are not independent, and their correlation is represented by the past events maps in Bevilacqua et al. (submitted).

The second model, called Model 2, samples the direction and distance independently. In other words, in Model 2 both the distances and the directions are based on past events maps, but we assume there is not a link between the direction of the projectiles and the distance they reach. Therefore, this model allows for combining distances and directions not as jointly observed in the past events. In this way it is possible to consider the effect of specific directional conditions that combine the average distance distribution with the most likely angular directions of dispersal. In Model 2, for every angle θ in [0, 360°], the ballistic direction probability, also reported in Figures 2c,d, is:

$$G(\theta) = |\{j : \theta \in \cup_i (\alpha_{ij} - W_{ij}/2, \alpha_{ij} + W_{ij}/2)\}|/N, \quad (2)$$

where α_{ij} and W_{ij} are the bisector azimuth and the width values of the i-th sector of the j-th explosion, and N is the total number of the explosions in the dataset.

For every $d > 0$, we define $F_A(d)$, reported in Figures 2a,b, as the exceedance probability function of the ballistic distances calculated by not including the proximal axisymmetric part, and $F_0(d)$ the exceedance probability function by only considering the axisymmetric part. Then, for every (d, θ) in the map, we define:

$$H^{(2)}(d, \theta) = F_A(d) \cdot G(\theta) + F_0(d) \cdot [1 - G(\theta)]. \quad (3)$$

https://doi.org/10.5194/egusphere-2025-6540
Preprint. Discussion started: 12 January 2026

The last model, called Model 3, simply considers the exceedance probability function of the ballistic distances in all directions. Therefore, in Model 3 we assume that the directions and the distances of the ballistics are independent and that the directions are uniformly distributed on a full angle. Thus, this model provides an averaged probability also towards the less accessible and possibly under recorded zones. In Model 3, for every d > 0, the exceedance probability function of the ballistic distances is calculated as:

$$F_B(d) = P\{ X > d \}, \quad \text{and} \quad X := D_{ij}, \tag{4}$$

where j is uniformly sampled in 1,…, N, and i is sampled among the number of sectors of explosion j-th, by including the proximal axisymmetric part and weighted in proportion to W_{ij} / 360°. In these expressions, N is the total number of the explosions in the dataset and W_{ij} is the width of the sector. For every (d, θ) in the map, we define:

$$H^{(3)}(d, \theta) = F_B(d). \tag{5}$$

Also the function $F_B(d)$ is reported in Figures 2a,b (cases with axisymmetric part included).

It should be noted that Model 2 and Model 3 redistribute the probabilities of Model 1: their probability values can be either lower or greater than the spatial frequency of past events. In particular, the total sum of the probabilities of Model 3 coincide by construction with those of Model 1, while the total sum of Model 2 can slightly differ, because the circular sectors are evaluated separately from the proximal axisymmetric parts. However, as better presented in the results section, the total difference between the sum of Model 2 and the sum of Model 1 (or 3) is, expressed in percentage, ca. -2% for major explosions, and +12% for the paroxysms, indicating relatively small variations.

Finally, in order to adopt a conservative and robust approach against possible particularly directional dispersal and data under-sampling in the least accessible areas, we have produced maps by considering the point wise maximum of the three Models (k=1,2,3), i.e.,:

$$H^{(M)}(d, \theta) = \max_{k=1,2,3} H^{(k)}(d, \theta). \quad , \tag{6}$$

We also adopted a doubly stochastic approach to account for the effect of the uncertainty of the ballistic dispersal maps generated (Bevilacqua, 2016). In particular, we considered the effect of the uncertain definition of distances and directions of ballistic dispersal during past explosions. By following the detailed descriptions in Bevilacqua et al. (submitted), the calculation of the probability maps was performed in a Monte Carlo simulation that randomly changes the simplified maps of past events. Such a procedure generates ensembles of probability maps, represented in terms of mean and 5th and 95th percentile values (Neri et al., 2015; Bevilacqua et al., 2017; Rutarindwa et al., 2019; Aravena et al., 2023).

3.2 Probabilistic combination of the two categories of major explosions and paroxysms

As presented above, the description of major explosions and paroxysms rely on two different datasets, i.e., Bevilacqua et al. (2023) for major explosions from 1970 to 2023, and Bevilacqua et al. (2020b) for paroxysms from 1879 to 2023. Therefore,

https://doi.org/10.5194/egusphere-2025-6540
Preprint. Discussion started: 12 January 2026

in the Results sections these two categories are initially treated separately in order to describe their associated hazard with respect to ballistics. We also produced a probabilistic combination of these two categories. This is justified by two main reasons: 1) the evidence that we cannot know *a priori* the type of the next future event and 2) the finding that the main parameters describing the ballistic dispersal, such as the distance, width and area distributions of the two categories are remarkably continuous, thus indicating the absence of a net separation between the two categories (Bevilacqua et al., submitted).

The combination of these two categories was done by estimating the relative frequency of major explosions and paroxysms using the data from the two catalogs. Specifically, the paroxysms accounted for $p_A = 7.3\%$ of events between 1970 and 2023, and for $p_B = 12\%$ of events between 2003 and 2023 (a more conservative estimate). These estimates have both been made after excluding all the uncertain major explosions, which would decrease the paroxysm percentage of ca. 1/3.

The difference between p_A and p_B is due to the fact that only 5 paroxysms occurred after 1970: their time series is irregular and characterized by temporal clusters and a 44-year gap between 1959 and 2003 (Bevilacqua et al., 2020a). Therefore, the fraction of the number of paroxysms over the number of major explosions drops down if we include the time interval between 1970 and 2003. However, the same ratio grows to ca. 19% if evaluated on the longer time interval from 1879 to 2023, even after we included all the uncertain major explosions (see Bevilacqua et al., submitted). Therefore, we assumed that $p_B = 12\%$ as a relatively robust and conservative estimate of this important scale parameter.

As a consequence, for every Model k=1,2,3,M, the combined model is defined as:

$$H^{(k,\,comb.)}(d,\theta) = p \cdot H^{(k,\,parox.)}(d,\theta) + (1-p) \cdot H^{(k,\,major\ exp.)}(d,\theta), \quad (7)$$

where p is equal to p_A or p_B.

We finally note that for the combined model M, which considers in each spatial point the maximum values between Model 1, 2 and 3 holds:

$$H^{(M,\,comb.)}(d,\theta) \geq \max_{k=1,2,3} H^{(k,\,comb.)}(d,\theta), \quad (8)$$

because the dominant model for the major explosions can differ from the dominant model for the paroxysms, depending on the location. In the following, we will always show the outcomes of the formulation $H^{(M,\,comb.)}(d,\theta)$.

https://doi.org/10.5194/egusphere-2025-6540
Preprint. Discussion started: 12 January 2026

4 Results

4.1 Ballistics probability maps of major explosions and paroxysms

Figure 4 shows the mean probability maps of ballistic projectiles fallout according to Models 1, 2 and 3, and by considering separately major explosions and paroxysms. All the maps represent the mean values with respect to epistemic uncertainty considered.

- Major explosions: Model 1 (Fig. 4a) describes the distribution of the ballistic particles as obtained from the reconstruction of past events. The probability curves clearly show a predominant dispersal towards NE. In more detail, the contours below 35% are all significantly asymmetric towards NE, on the slopes above 400 m a.s.l, whereas the contours over 35% are slightly asymmetric towards SE, on the upper portion of Rina Grande. In Model 2 (Fig. 4c), the distribution of probability is significantly different from that of Model 1 and all contours are asymmetric towards SE, affecting the whole Rina Grande area above 400 m a.s.l.. Finally, Model 3 (Fig. 4e) assumes an axisymmetric distribution of the area affected by ballistics. In this case the 35% contour is over ca. 700 m elevation except towards Sciara del Fuoco. A notable difference between the three models is that the trails at 600 m elevation to the NE of the summit, over 750 m from the craters, are affected 10% of the times under Model 2 and Model 3, and ca. 20% according to Model 1.

- Paroxysms: in Model 1 (Fig 4b) all the probability contours are asymmetric towards NE and WSW, with the 35% contours enclosing regions at ca. 300 m a.s.l. above Ginostra and Stromboli villages. Contours up to 10-20% also affect the village of Ginostra whereas the village of Stromboli is affected by probabilities between 2 and 5%. For Model 2 (Fig. 4d) all the contours above 35% are widely asymmetric towards N with the 35% contour enclosing similar zones to Model 1, but also the entire Sciara del Fuoco; Ginostra experiences values between 5 and 10%. Finally, Model 3 (Fig. 4f) is symmetrically distributed with the 35% contour at 500 m a.s.l. towards NE and WSW (above the villages) and at ca. 700 m a.s.l. to the S; the 2% contour includes the whole island with the only exception of the most NE part of the Stromboli village. Again, some major differences are evident between the three Models: for example, Ginostra village, over 1750 m from the craters, is affected 2-5% of the time under Model 3, 5-10% according to Model 2, and even above 20% by assuming Model 1, on average.

Figure 5 shows in more detail the differences between the mean probability maps of ballistic projectiles after Model 1, 2 and 3, for both major explosions and paroxysms. Regarding major explosions, Figures 5a,c,e, illustrate that Model 1 dominates towards the NE direction, Model 2 dominates towards the SE direction, whereas Model 3 dominates towards W. In all cases the differences between all pairs of Models are up to ca. 15%.

As regards the paroxysms, Figure 5b,d,f, show that Model 1 dominates towards NE and WSW, Model 2 mostly dominates towards NW, i.e., in the Sciara del Fuoco, whereas Model 3 mostly dominates towards S. Also for paroxysms, the differences in the mean values between each pair of Models are also up to ca. 15%.

https://doi.org/10.5194/egusphere-2025-6540
Preprint. Discussion started: 12 January 2026

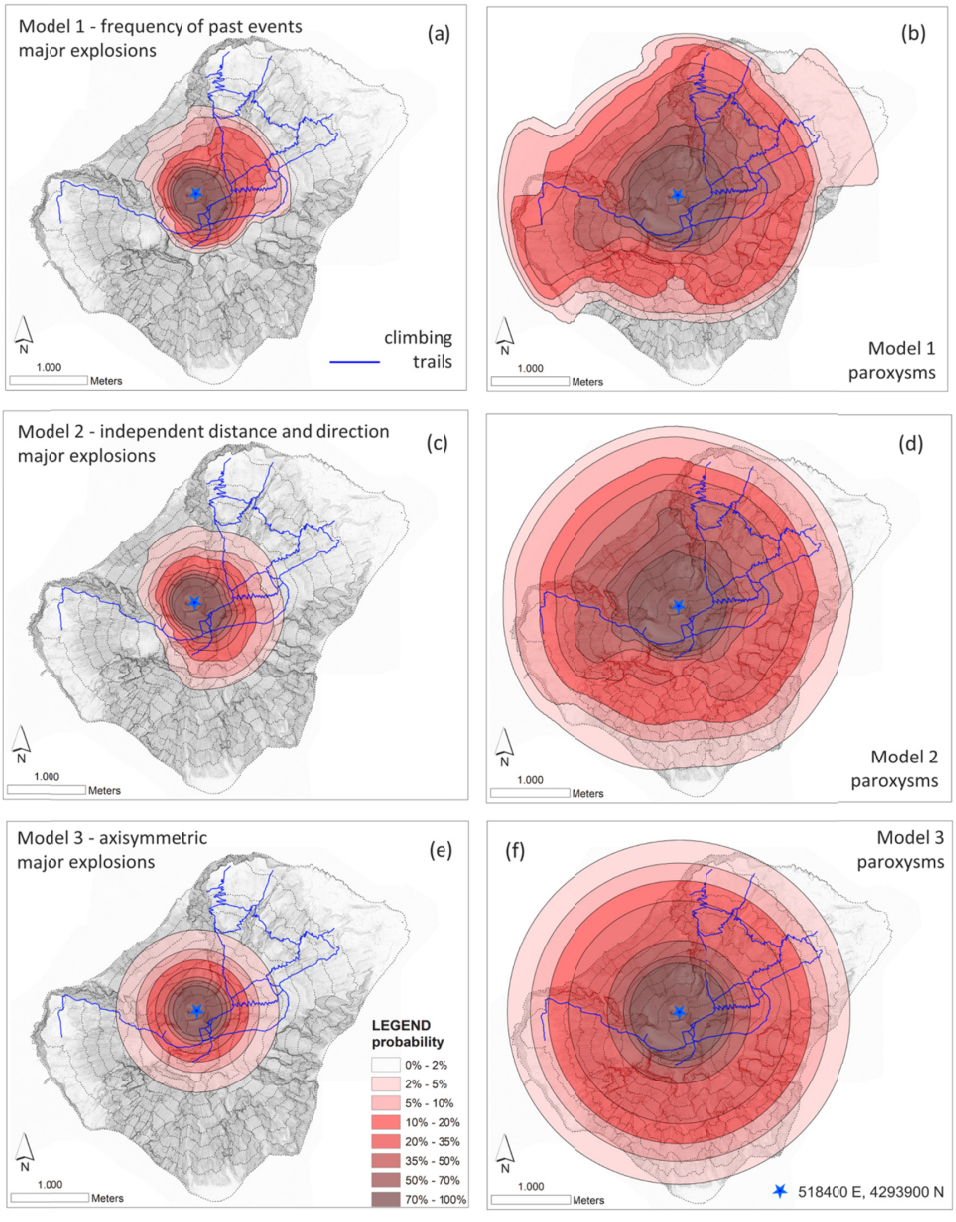

Figure 4: Mean probability maps of ballistic projectiles from major explosions (a,c, e) and paroxysms (b,d,f). In (a,b) Model 1 is applied, in (b,c) Model 2 and in (e,f) Model 3. Estimates are conditioned on the occurrence of either a major explosion or a paroxysm, respectively. Colors and contour lines indicate percentage values. In the background is a vertical shaded relief map.

https://doi.org/10.5194/egusphere-2025-6540
Preprint. Discussion started: 12 January 2026

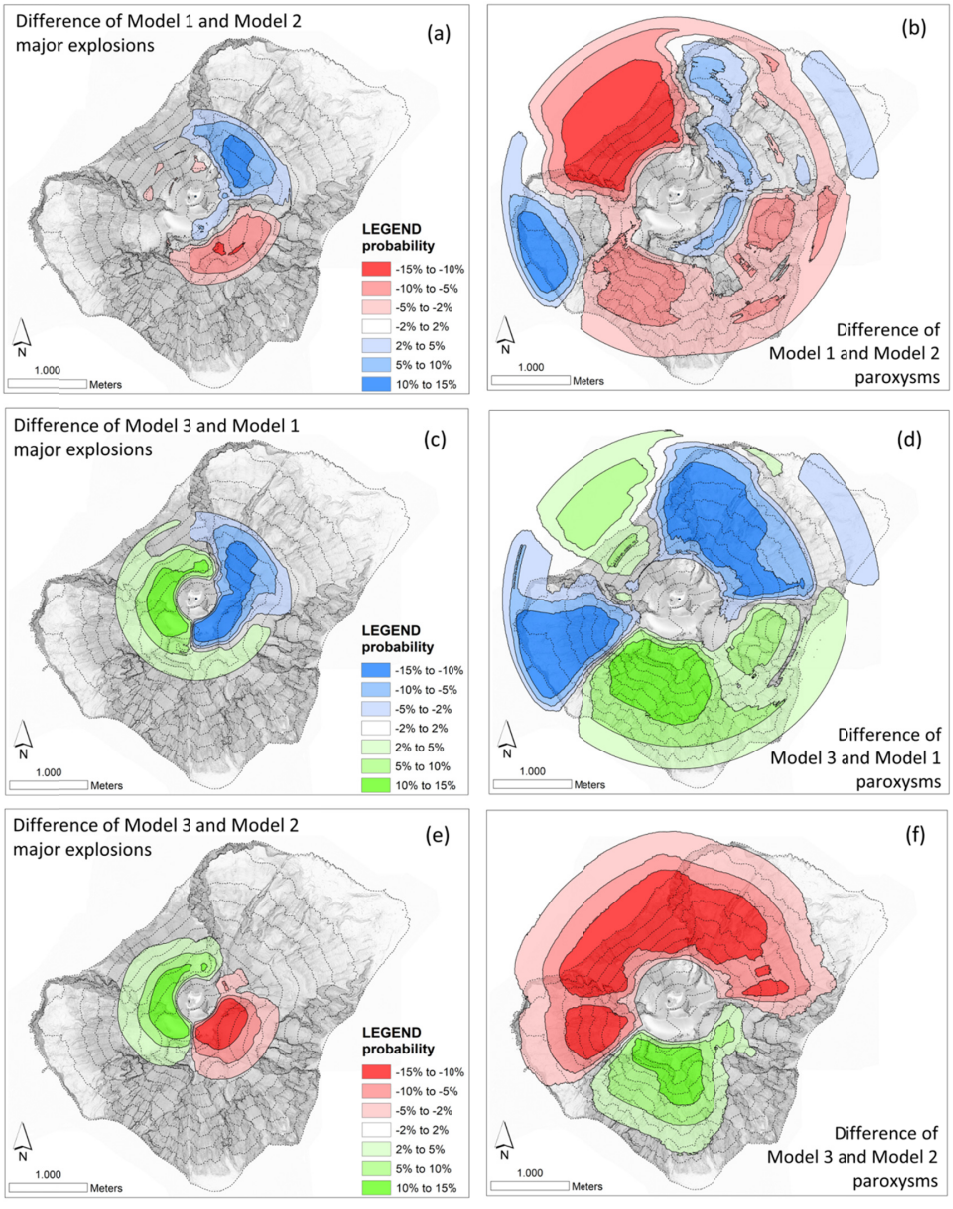

290

Figure 5: Difference between mean probability maps of ballistic projectiles: (a,b) are Model 1 minus Model 2, (c,d) are Model 3 minus Model 1, and (e,f) are Model 3 minus Model 2. (a,c,e) are related to major explosions, and (b,d,f) to paroxysms. Colors and contour lines indicate differences in percentage values. In the background is a vertical shaded relief map.

https://doi.org/10.5194/egusphere-2025-6540
Preprint. Discussion started: 12 January 2026

Figure 6 and Figure 7 show the mean values and the 5th and 95th percentile values probability maps of ballistic projectiles from major explosions and paroxysms, respectively, according to the doubly stochastic formulation described in subsection 3.1. These maps refer to the maximum values between Models 1, 2, and 3, i.e., $H^{(M)}(d, \theta)$ as in Eq. (6).

In the mean map of major explosions, shown in Figure 6a, the 10% contour is asymmetrical towards E, and particularly towards NE, enclosing the slopes above Stromboli village above ca. 450 m a.s.l. and the Rina Grande above ca. 550 m a.s.l.. However, the 2% contour is almost symmetrically distributed with a radius of about 1 km and just a minor asymmetry in the E halfplane.

In the mean map of paroxysms, presented in Figure 7a, instead the 10% contour encloses the lower slopes above Stromboli village at ca. 100 m a.s.l., and, towards WSW, almost the entire Ginostra village is affected by probability above 20%. Moreover, during the paroxysms, the sea in front of Sciara del Fuoco is affected ca. 40% of the times near the shoreline, and ca. 5% at 1 km distance offshore.

Finally, it is worth noting that the estimated uncertainty on the reconstructed areas affected by ballistics, has a rather limited effect on the probability isolines of both major explosions and paroxysms: in fact the 95th percentile contours are ca. 150 m (Figures 6b and 6c) and ca. 250 m (Figures 7b and 7c) larger than the equivalent 5th percentile contours, for the two categories, respectively.

Table 1 summarizes the mean values of the probability to be affected by ballistics in a list of ten areas of the island at different distances and directions from the craters. These are touristic or populated areas, or crossed by one of the main climbing trails. Namely, we consider, the NE trails at 600 m a.s.l., Labronzo trail at 400 m, 290 m and 100 m a.s.l., Stromboli village, Ginostra trail at 450 m a.s.l., Ginostra village, upper and lower Rina Grande area, Forgia Vecchia beach (Fig1 b).

https://doi.org/10.5194/egusphere-2025-6540
Preprint. Discussion started: 12 January 2026

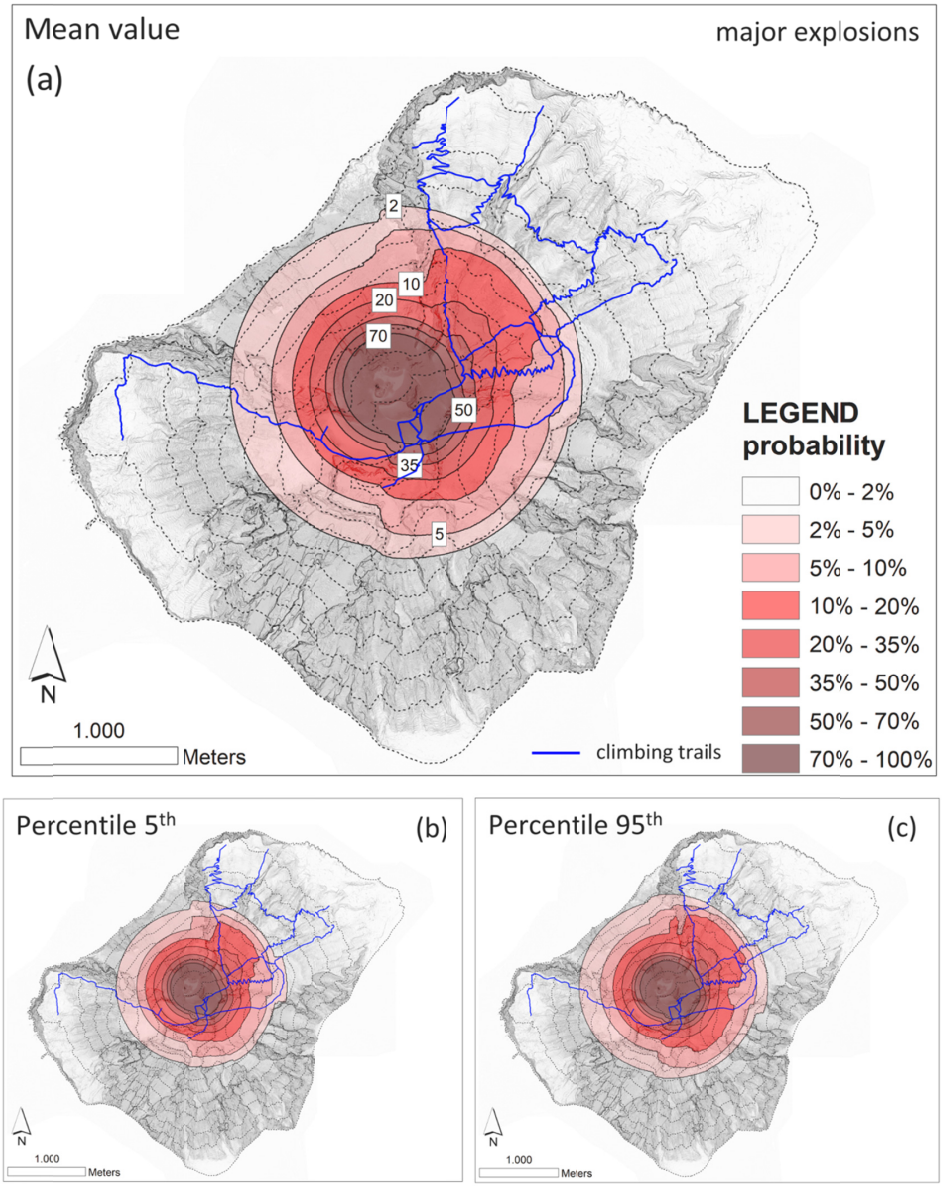

Figure 6: (a) Mean and (b,c) 5th and 95th percentiles probability maps of the areas affected by ballistic projectiles fallout from major explosions assuming in each spatial point the maximum values between Model 1, Model 2, and Model 3. Estimates are conditioned on the occurrence of a major explosion. Colors and contour lines indicate percentage values as shown in the legend. In the background is a vertical shaded relief of the island.

https://doi.org/10.5194/egusphere-2025-6540
Preprint. Discussion started: 12 January 2026

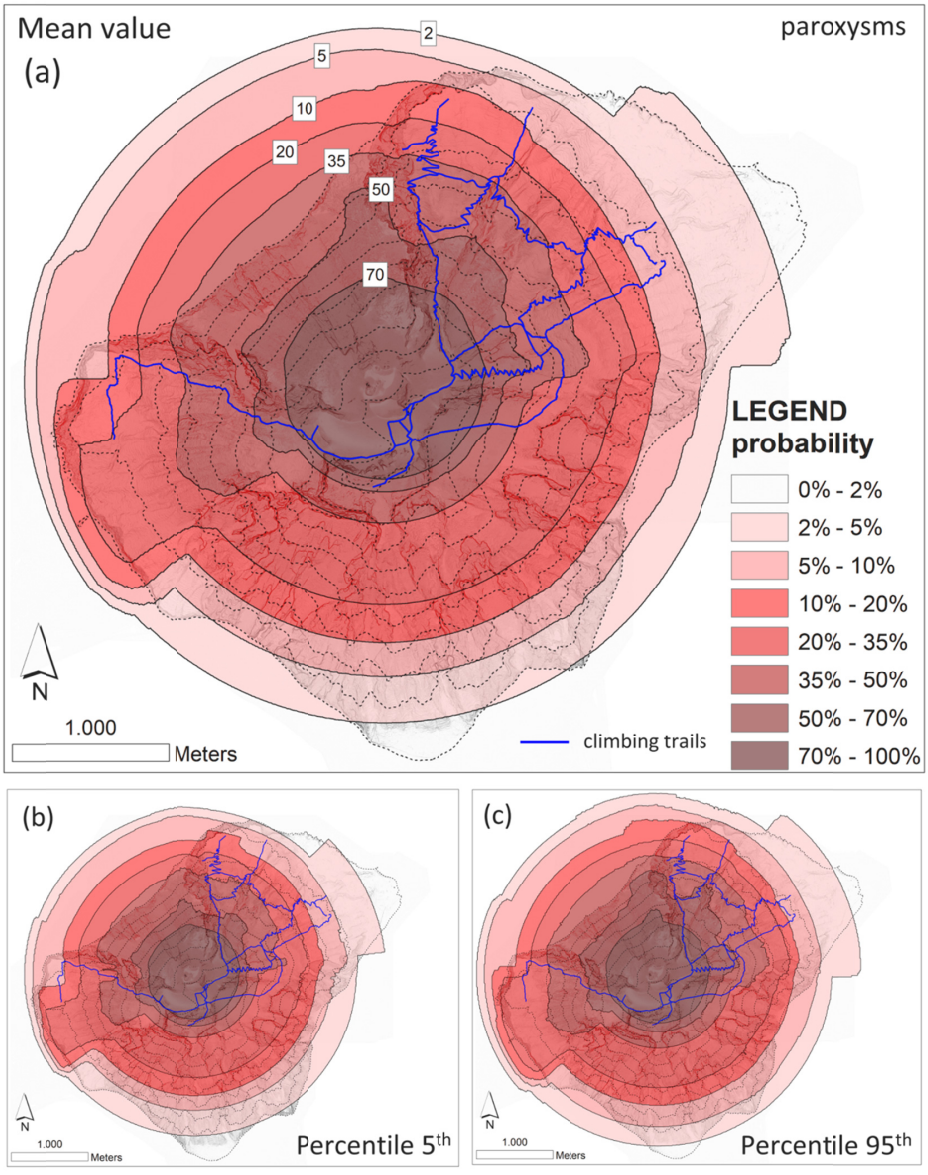

Figure 7: (a) Mean and (b,c) 5th and 95th percentiles probability maps of the areas affected by ballistic projectiles fallout from paroxysms assuming in each spatial point the maximum values between Model 1, Model 2, and Model 3. Estimates are conditioned on the occurrence of a paroxysm. Colors and contour lines indicate percentage values as shown in the legend. In the background is a vertical shaded relief of the island.

https://doi.org/10.5194/egusphere-2025-6540
Preprint. Discussion started: 12 January 2026

Table 1: Summary of main probability values to be affected by ballistic fallout for different areas of Stromboli as derived by the presented probability maps. The numbers reported from Figures 6-8 and S3 are the approximate mean values with respect to the considered uncertainty. The numbers referred to Figures 10 and S4 are the uncertainty interval between the 5th percentiles of Fig. S3 and the 95th percentiles of Figure 8. For locations see Fig. 1b.

	North and NE flanks					West flank		SE flank		
	NE trails, 600 m a.s.l.	Labronzo trail, 400 m a.s.l.	Labronzo trail, 290 m a.s.l.	Labronzo trail, 100 m a.s.l.	Stromboli village	Ginostra trail, 450 m a.s.l.	Ginostra village	Rina Grande, 750 m a.s.l.	Rina Grande, 500 m a.s.l.	Forgia Vecchia beach
Distance from the craters Direction from the craters	750 m NE	1100 m N	1300 m N	2000 m N	2000 m NE	1000 m W	1750 m WSW	500 m SE	1000 m SE	1750 m ESE
Fig. 6 - Mean ballistics Probability in case of major explosion	20%	3%	-	-	-	3%	-	50%	5%	-
Fig. 7 - Mean ballistics Probability in case of paroxysm	65%	45%	35%	10%	2%	45%	20%	70%	35%	10%
Fig. 8 - Mean ballistics probability in case of major explosion or paroxysm (parox. 12%)	25%	8%	5%	1%	<< 1%	7%	3%	54%	9%	1%
Fig. S3 - Mean ballistics probability in case of major explosion or paroxysm (parox. 7.3%)	20%	6%	3%	< 1%	<< 1%	6%	1.5%	51%	8%	< 1%
Fig. 10 and S4 - Ballistics probability in case of major explosion or paroxysm (90% uncertainty interval)	18% to 28%	5% to 11%	2.5% to 5%	< 1%	<< 1%	4% to 8%	1.5% to 3.5%	48% to 60%	6% to 10%	< 1% to 1.5%

https://doi.org/10.5194/egusphere-2025-6540
Preprint. Discussion started: 12 January 2026

4.2 Ballistics probability maps and curves combining major explosions and paroxysms

According to the combination formula (Eq. 7) in Subsection 3.2, Figure 8 shows the mean value and the 5th and 95th percentile probability maps of ballistic projectiles from major explosions and paroxysms considered together, i.e. as a single category. Specifically, in Figure 8 the paroxysms account for 12% of events, the remaining 88% of events being major explosions, as observed during the last two decades of activity, i.e. between 2003 and 2023 (see Bevilacqua et al., submitted). It is noteworthy that contour lines extend now to minimum values of 1% (against the 2% value adopted for the two separate categories) given the larger number of events considered in producing the combined map.

In the combined mean map, the 10% contour is asymmetrically distributed towards E and particularly towards NE, enclosing the slopes above Stromboli village above 400 m a.s.l., Rina Grande and the area above Ginostra above 500 m a.s.l.. In contrast, the 2% contour is asymmetrical towards WSW, enclosing the entire Ginostra village up to the harbor, the sea in front of Sciara del Fuoco up to about 600 m offshore, and the slopes above Stromboli village at ca. 200 m a.s.l. These different patterns of the higher and lower contour lines clearly reflect the remarkably different features of major explosions and paroxysms, with the former dominating in the most proximal areas and the latter in the distal ones.

As for the maps shown in Figs. 6 and 7, the effect of the uncertainty is limited also for the combined map. The 95th percentile contours are up to ca. 150 m more distant from the craters than the 5th percentile contours in the upper portion of the island, exposed to both the major explosions and the paroxysms, whereas they are up to ca. 250 m larger in the lower portion, which is only exposed to paroxysms.

In Supplementary Figure S3 we reported the combined maps of the paroxysms account for just 7.3% of events, as computed considering the more extended period of activity between 1970 and 2023, with less than 5% probability reduction in the considered areas, if compared to the corresponding values shown in Figure 8. See Table 1 for a summary of the probability values associated to these combined maps.

https://doi.org/10.5194/egusphere-2025-6540
Preprint. Discussion started: 12 January 2026

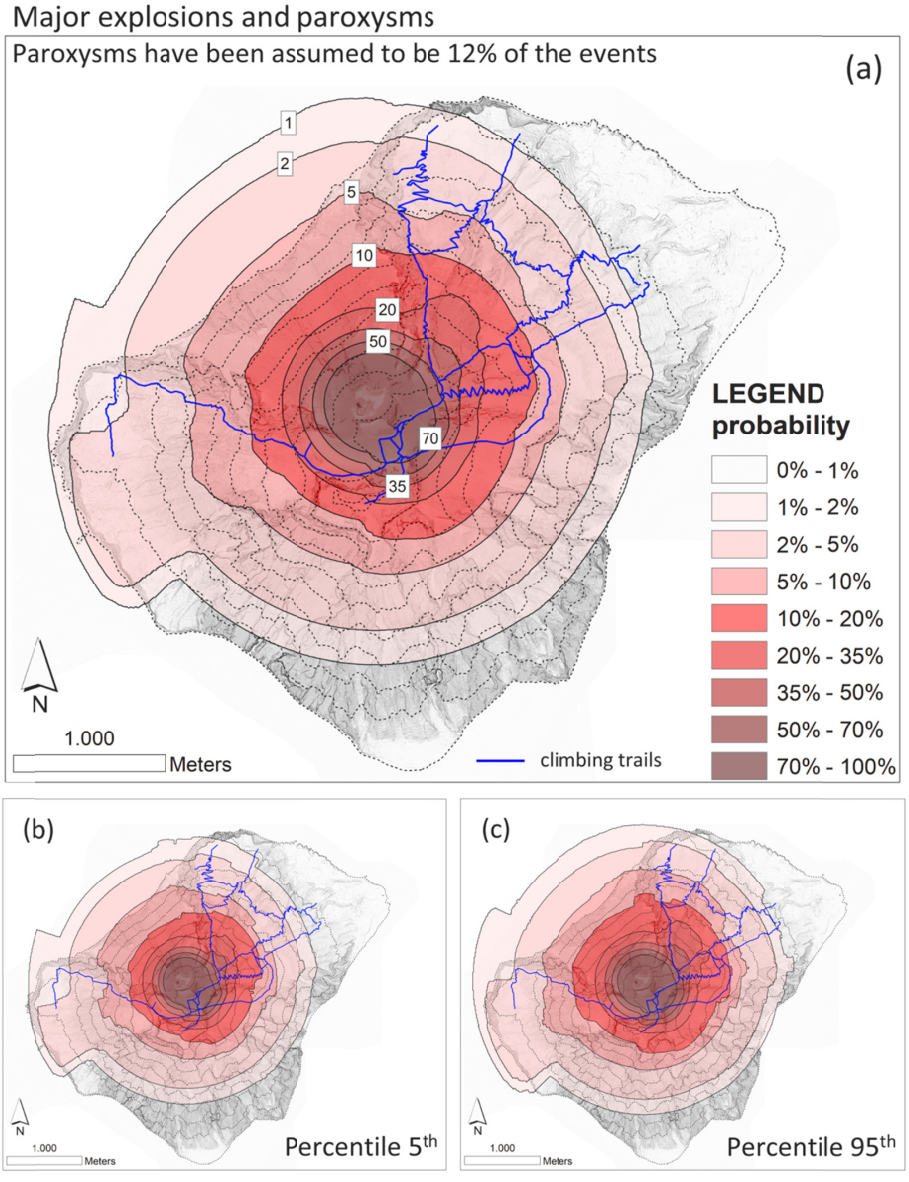

Figure 8: (a) Mean and (b,c) 5th and 95th percentile probability maps of the areas affected by ballistic projectiles fallout from major explosions and paroxysms, based on event count from 2003 to 2023. Estimates are conditioned on the occurrence of a major explosion or a paroxysm with relative probabilities of 88% and 12%, respectively. Maximum values between Models 1, 2, and 3 are assumed in each location. Colors and contour lines indicate percentage values as shown in the legend. In the background is a vertical shaded relief of the island.

https://doi.org/10.5194/egusphere-2025-6540
Preprint. Discussion started: 12 January 2026

It is also informative to analyze the distribution of ballistic hazard at specific distances from the craters and specific elevations. Figure 9 shows the probability curves of ballistic hazard from major explosions and paroxysms, considered as a single category, as a function of direction from the center of the Crater Terrace, at six selected distances from the craters. These curves report the Maximum Model values shown in Figure 8a (as mean value) and also those calculated by Models 1, 2, and 3, along the selected isolines of distance and parameterized with respect to the azimuth angle. Their comparison highlights the importance of having considered multiple models. In fact, for each distance isoline, depending on the direction, the dominant model can be any of the three depending on the specific features of each model for that direction. We also note that in a few cases, the maximum values are slightly greater than all the three models, because the dominant model for the major explosions can differ from the dominant model for the paroxysms. Supplementary Figures S5 and S6 similarly report the major explosions and the paroxysms probability curves separately.

Similarly, Figure 10 and Supplementary Figure S4 show the mean probability hazard curves of Fig. 8 and S3 as a function of direction, at six selected distances from the craters, and six elevations a.s.l., respectively. Specifically, they report the mean values of Figures 8 and S3, and the uncertainty interval between the 5^{th} percentiles of Fig. S3 and the 95^{th} percentiles of Fig. 8. This analysis complements the probability values computed at the locations listed in Table 1. For example from Figure 10b, at 150 m elevation, there is 1.5% to 3% probability on the Labronzo trail, and 2% to 4% in the cultivated fields above Ginostra. Similarly, from Figure S4d, at 1000 m from the craters, there is a peak probability of 11% to 17% at ENE, in the area where the climbing trail exits vegetation (see Fig. 1b).

https://doi.org/10.5194/egusphere-2025-6540
Preprint. Discussion started: 12 January 2026

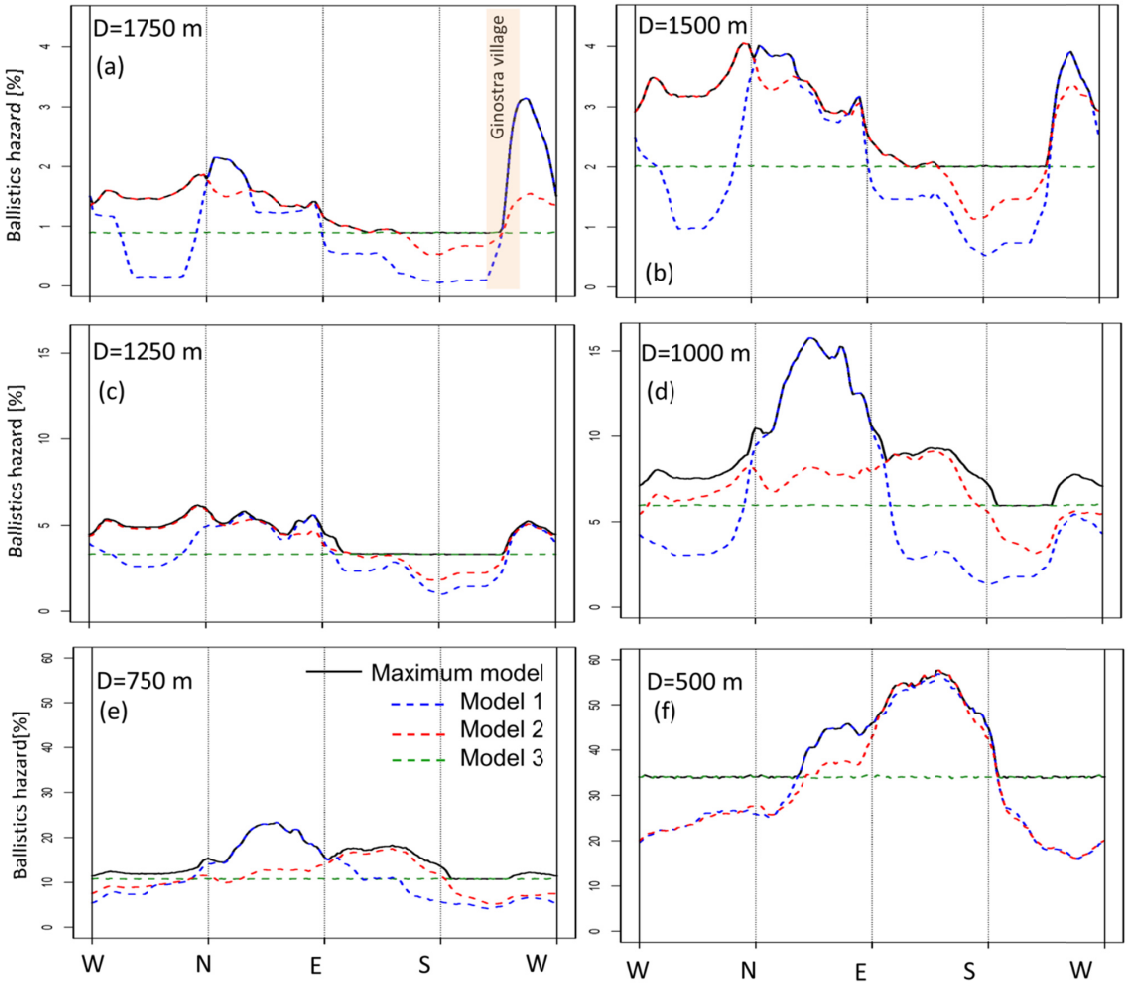

Figure 9: Probability curves of ballistic hazard from major explosions and paroxysms, considered as a single category, as a function of direction from the center of the Crater Terrace, at six selected distances from it (see Fig. 1a for the location of the corresponding distances). The plots show the curves of the Maximum Model values (black curve) compared to those of Models 1 (blue dashed), 2 (red dashed), and 3 (green dashed). The plots refer to mean values with respect to the uncertainty and assume, in this example, a relative weight of paroxysms of 12% with respect to the total explosive events considered (major explosions and paroxysms). In panel (a), the direction of Ginostra village is highlighted in pink. Note the different scales reported on the ordinate of the different plots.

https://doi.org/10.5194/egusphere-2025-6540
Preprint. Discussion started: 12 January 2026

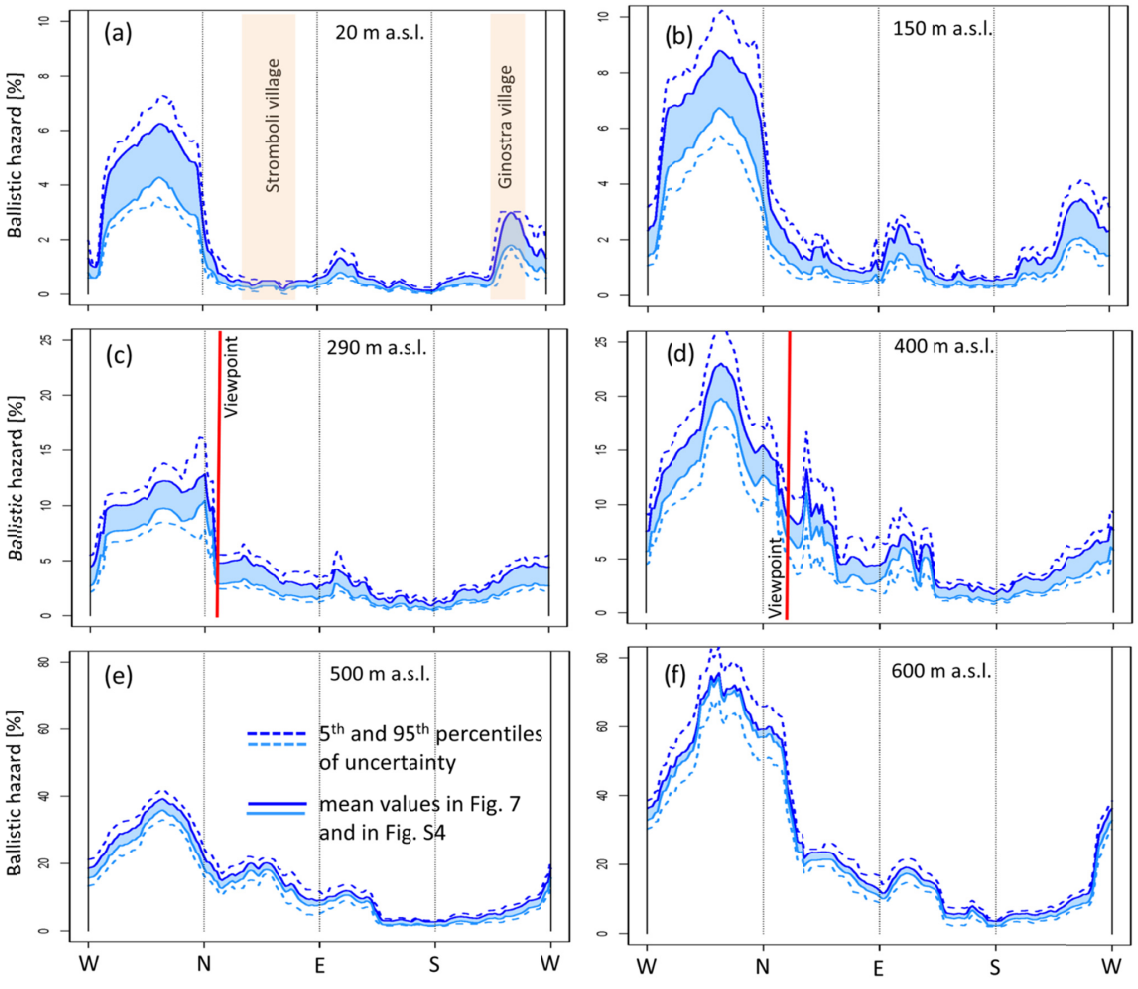

Figure 10: Probability curves of ballistic hazard from major explosions and paroxysms, considered as a single category, as a function of direction from the center of the Crater Terrace, at six selected elevations a.s.l. (see Fig. 1b for the location of the corresponding isoipses). All curves refer to the Maximum Model values between Models 1, 2, and 3. The uncertainty interval between the two continuous curves refers to the choice of the relative weight of paroxysms, either 7.3% or 12%, as discussed in the text. The dashed curves indicate the 5th and 95th percentiles of the uncertainty. In panel (a), the directions of the two inhabited areas of Stromboli and Ginostra villages are highlighted in pink, in panels (c,d) the directions of the viewpoints on the Labronzo trail are shown as vertical red lines (see Fig. 1). Note the different scales reported on the ordinate of the different plots.

https://doi.org/10.5194/egusphere-2025-6540
Preprint. Discussion started: 12 January 2026

4.3 Temporal occurrence model and spatio-temporal ballistic hazard estimates

All the hazard estimates presented in the previous sections were conditional on the occurrence of a major explosion or a paroxysm. To account for the time variable, it is necessary to assume a temporal model, in order to consider the probabilities of occurrence of major explosions and paroxysms. In Bevilacqua et al. (2020a), a two-state Markov chain was able to replicate the clustering features of major explosions and paroxysms at Stromboli, by fitting the bulk of the inter-event times with an exponential and the tail with a lognormal distribution. In fact, a constant probability rate of events, i.e., a Poisson model, was inadequate to estimate these clustered events. Supplementary Figure S7 reports the hourly probabilities of the major explosions and paroxysms as a combined class, and only of paroxysms. It should be noted that the probability of occurrence models can be either fitted by excluding the uncertain major explosions, or including them in the count, thus producing different results (Bevilacqua et al., 2020a).

The probability rates of major explosions and paroxysms are not constant in time, but significantly increase in the weeks/months after one of these events has occurred. In particular, based on Figure S7, after including the uncertain major explosions, the hourly probability of major explosions and paroxysms is ≈0.05% in the first weeks after the event, but gradually decreases below 0.025% in ca. 3 months. Similarly, the hourly probability of paroxysms is ≈0.013% in the first months after the event, and then decreases below 0.0025% in ca. 15 months. These results refer to the currently analyzed eruption record, but they are broadly consistent with those reported in Bevilacqua et al. (2020a).

Figure 11 summarizes four examples of ballistic hazard maps using different hourly probabilities, i.e. representative of the hazard after specific time periods from the last explosive event. In Figure 11a we used 0.05%, i.e., the “peak” hourly probability estimated after about 15 days of the last major explosion or paroxysm; in Figure 11b we assumed 0.025%, as estimated after 3 months without major explosions or paroxysms. It should be noted that the mapped values are the product of Figure 8 and the hourly probabilities mentioned above, and therefore the values in Figure 11a are twice of those in Figure 11b. Moreover, because the hourly probability of the paroxysms shows an increase lasting for over a year after every event of that type, in Figure 11c and 11d we modified the previous maps by assuming 0.013% hourly probability only for the paroxysms. In practice, in Figures 11c and 11d we considered the maximum value between Figure 11a and 11b, respectively, and the product of Figure 7 and 0.013% hourly probability of occurrence. These two maps report greater probabilities than the previous pair, especially in the lower portions of the island, i.e., below 400 m a.s.l.. Simplifying, Figure 11a and 11b are representing the ballistic hazard if no paroxysm occurred in the previous few months; Figure 11c and 11d are valid in the few months after a paroxysm occurred. It should be noted that the peak hourly probability values in Figure S7 are greater than 0.05% in the first few days after the last explosive event.

After the hourly probabilities, the probabilities of the areas affected by ballistic projectiles of at least one major explosion or paroxysm in the next 10 or 50 years are also relevant, particularly in the inhabited areas. For all spatial coordinates (x,y) we calculated the ballistic fallout probability for the next N years by using the following equations:

https://doi.org/10.5194/egusphere-2025-6540
Preprint. Discussion started: 12 January 2026

$$H_N(x,y) = \Sigma_j P_{N,j} [1 - (1 - H(x,y))^j], \quad (9)$$

where the index j = 1, …, k parameterizes the number of major explosions or paroxysms that may occur, $P_{N,j}$ is the probability to have exactly j such events over the next N years, and H(x,y) is the conditional probability of the areas affected by ballistic fallout.

Figure 12 shows two examples of ballistic hazard maps from major explosions and paroxysms, considered as a single category, in the next 10 years, based on a MC simulation of 500,000 samples of the number of major explosions and paroxysms that may occur. In particular, Figure 12a excludes the uncertain major explosions, and Figure 12b includes them in the occurrence probability estimates: in the Stromboli Village we calculated probabilities up to 5% in Figure 12a and up to 10% in Figure 12b, whereas in Ginostra we calculated probabilities up to 35% and up to 50%, respectively. Figure 12c shows the probability distribution of the number of major explosions and paroxysms that we considered in the next 10 years, and a similar estimate for the next 50 years. It should be noted that, after including the uncertain major explosions, mean values are 23.5 of these events in the next 10 years, and ca. five times more, 117, in the next 50 years, of which ca. 88% would be expected to be major explosions and 12% to be paroxysms, according to the event ratio assumed in Figure 8.

https://doi.org/10.5194/egusphere-2025-6540
Preprint. Discussion started: 12 January 2026

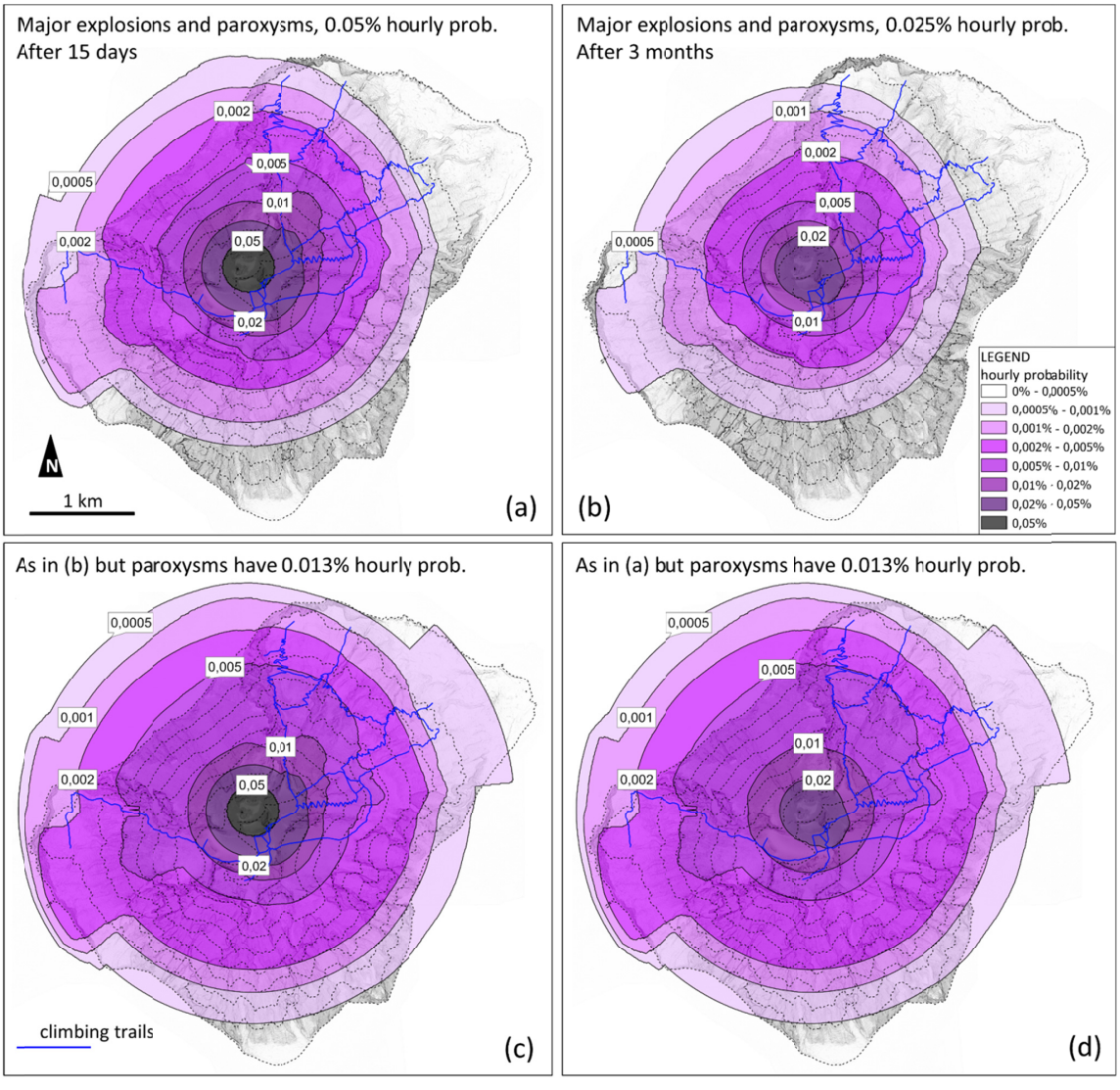

Figure 11: Hourly probability maps of the areas affected by ballistic projectiles of major explosions and paroxysms after (a,c) 15 days and (b,d) 3 months from the last event. All estimates are based on Figure 8 but assuming different occurrence probabilities. In (a) we assumed 0.025% and in (b) 0.05% hourly probability of major explosions and paroxysms considered as a combined class. In (c) and (d) we modified (a) and (b), respectively, by incrementing the occurrence probability of only the paroxysms to 0.013%. Colors and contour lines indicate percentage values as shown in the legend. In the background is a vertical shaded relief of the island.

https://doi.org/10.5194/egusphere-2025-6540
Preprint. Discussion started: 12 January 2026

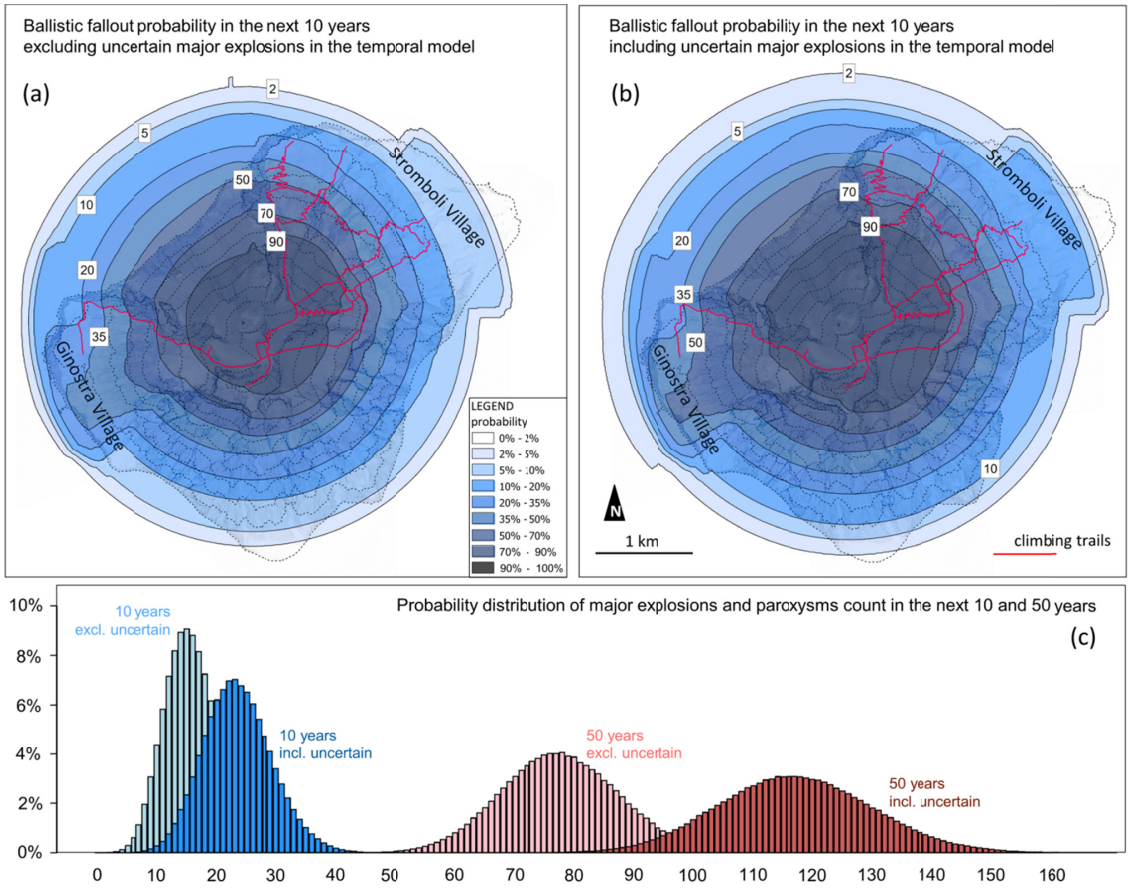

Figure 12: (a,b) Probability maps of the areas affected by ballistic projectiles of at least one major explosion or paroxysm in the next 10 years, based on the number of (c) the probability distribution of the number of major explosions and paroxysms considered as a combined class. In (a) we exclude the uncertain major explosions, and in (b) we include them in the occurrence probability estimates. We adopt a Monte Carlo simulation of the occurrence probabilities reported in Supporting Figure S7a and S7b, respectively.

.

https://doi.org/10.5194/egusphere-2025-6540
Preprint. Discussion started: 12 January 2026

5 Discussion

5.1 Ballistic hazard estimates at Stromboli

The ballistic fallout hazard estimates in the existing scientific literature started with qualitative maps mostly informed by the areas of heavy ballistic fall described in 1930 (Nappi, 1977; Capaldi et al., 1978). Then, Barberi et al. (1993) by leveraging on their pioneering historical catalog, improved on this, by outlining five hazard zones affected by different volcanic hazards in the past. Four of these zones were related to ballistic hazard, enveloping the region above 400 m a.s.l. plus some of the island flanks down to the coastline. In Rosi et al. (2013) two qualitative maps were presented, the first related to the probability of ballistic fallout of blocks during major explosions, and the second to the probability of ballistic fall in general, including "spatter" fallout and hot avalanches related to the paroxysms. Both maps were informed by the field data from a small number of events, namely six major explosions and three paroxysms. The former map roughly corresponded to a circular sector oriented towards NE, with hazard modulated from high to low in terms of distance from the craters and main topographic basins. The latter map delineated a wide sector, from SSW to NNW clockwise, were ballistic hazard was considered high from the coastline to the summit, plus a few hundreds of meters offshore Sciara del Fuoco; on the rest of the island the ballistic hazard ranged from low to high as a function of elevation a.s.l.. It should be noted that both these maps established qualitative hazard rankings, ranging from low to high, without assigning any numerical values.

In this study we developed a new method implementing complementary models to estimate probabilistically the areas affected by ballistic projectiles during the major explosions and paroxysms at Stromboli, including the less accessible sectors of the island. We quantified probability values informed by a new dataset of 67 of these events and their uncertainty. First we directly used the reconstructed areal data as reported in the companion manuscript (Bevilacqua et al., submitted), i.e., at each point on the island we estimated the percentage of cases in which ballistic fallout affected that point (we called this Model 1). Then, we modeled the categorized dispersal areal data, i.e., distance, azimuthal direction and width angles of the circular sectors representing the ballistic fallout of past events. The existence of correlation structures characterizing the categorized data is evident from Figures 2 and 3, but it is unclear if they have been mostly caused by characteristics in the morphology of craters and shallow part of conduits, which likely change from time to time and become different in the future, or also by sampling biases.

The main advantage of using categorized data was the possibility to model distances and directions independently, still assuming that some directions were more likely affected than others, according to what observed in the available data. Therefore, the marginal distribution of the distances ($F_A(d)$) was calculated from the statistics of all the sectors, regardless of their direction (we called this Model 2). Finally, we also dropped the assumption that some directions were more likely than others and followed an axisymmetric assumption, by using the marginal distribution of all the observed distances ($F_B(d)$) uniformly in all directions (we called this Model 3). We believe that such a multi-model and conservative approach, although

https://doi.org/10.5194/egusphere-2025-6540
Preprint. Discussion started: 12 January 2026

still firmly based on past data and observations, significantly enhances the robustness of the hazard maps against possible under-recording issues and unstationary behavior of the volcanic system.

5.2 Considerations on the areal density of the ballistic projectiles

A remarkable aspect of the study is that we referred to the probability that a given area would be affected by ballistic fallout if a major explosion or a paroxysm occurs. In other words, in our analysis we did not consider the areal density of the projectiles. In fact, although there is a remarkable record of scientific articles and eyewitness descriptions of the products of major explosions and paroxysms in the past ca. 150 years (Bevilacqua et al., submitted), the number of projectiles per unit area was rarely reported and therefore it is difficult to evaluate. Unseen, unnoticed, or fragmental projectiles pose a major challenge to such measurements. In practice, witnesses often struggled to provide precise data, meaning that only the largest or most destructive projectiles tend to be reported.

Estimates of the areal density of ballistics are indeed quite rare and partial. Just for the most recent major explosions, a few field surveys locally measured the areal density of clasts, in terms of number of projectiles per meter square. They are listed in Supporting Table S1, and the peak densities range from 0.01-0.04 to 10-15 clasts/m^2 at distance of 300-500 m from the craters (e.g., Andronico and Pistolesi, 2010; Gurioli et al., 2013; INGV reports summarized in Bevilacqua et al., submitted). Schmid et al. (2025) reported a photogrammetric reconstruction of the ballistic fallout in the most proximal areas of the major explosion of 13 May 2022, identifying 20 scoriaceous bombs and more than 2,000 lithic blocks dispersed less than 250 m from the center of Crater Terrace. They did not quantify the areal density of the ballistics, but indicated several patches of continuous cover extending up to ca. 20 m of diameter.

Similarly, for paroxysms, the most studied event in terms of areal density of projectiles was the event of July 3, 2019. Notably, a continuous ballistic deposit was documented up to 350 m in the NE direction from the craters (Giordano and De Astis, 2021), and up to ca. 850 m in the WSW direction (i.e., 500 m a.s.l., Andronico et al., 2021). An areal density of 0.25 clasts/m^2 was observed 400 m NE from the craters, and one of 0.01-0.04 clasts/m^2 was observed at ca. 1800 m WSW (i.e., 100 m a.s.l., Andronico et al., 2021). In addition, for this paroxysm, detailed information on the areal density towards E was provided in Bisson et al. (2023), from an aerial survey performed six days after the paroxysm. In particular, they mapped up to 1.2 clasts per meter square at ca. 350 m from the craters, deemed equivalent to ca. 30% ground cover; they also measured a ground cover over 10% in the upper Rina Grande Area, ca. 500 m from the craters. On the W flank, Bevilacqua et al. (2024a) measured a ground cover up to 12% at ca. 900 m from the craters.

As a consequence, the areal density of ballistics during major explosions and paroxysms can be highly variable as a function of distance, diameter of the projectiles, and azimuthal direction: local clusters can also significantly diverge from the average measurements (Gurioli et al., 2013; Breard at al., 2014). Moreover, given an areal density of projectiles, the actual ballistic exposure of an individual target is hard to estimate, i.e., the probability of being struck. From a hazard perspective, any density above 1 clast per meter square is not different from a continuous cover (Jolly et al., 2014; Deligne et al., 2018). In

https://doi.org/10.5194/egusphere-2025-6540
Preprint. Discussion started: 12 January 2026

fact, while a complete ballistics exposure calculation should take into account the trajectory of the projectiles and their diameter (Jolly et al., 2014; Deligne et al., 2018), it is also the case that for these ballistic missiles there are no established injury thresholds for striking the head or other parts of the body, and their relatively low impact energies, i.e., 40 - 120 J, may even cause lacerations and skull trauma, depending on their shape and angle of strike (TNO, 1992; Davies, 1993; Baxter and Gresham, 1997). Then, it should be noted that even a slight areal enlargement, e.g., a buffer related to hot fragments affecting the surroundings, can produce a significant increase of the total area impacted by ballistics (Bevilacqua et al., 2024a), in particular, blocks falling on hard rock may fragment upon impact, sending dangerous shards as far as several tens of meters from the impact site (Rittmann, 1931; Rosi et al., 2006). For all these reasons, although we did not include the clast density in our analysis and our estimates cannot be considered as a measure of the probability to be struck by a ballistic fragment, they are certainly representative of the presence of a major risk in the area. Primary blast injuries can be excluded in Stromboli's explosions as their pressure waves are of a low order.

5.3 Uncertainty affecting the major-explosions/paroxysms ratio

An additional key parameter for the hazard assessment of major explosions and paroxysms at Stromboli is the fraction p of the number of paroxysms over the number of major explosions plus paroxysms, which we assumed equal to 12% in Figure 8, and equal to 7.3% in Figure S3, as discussed in the Methods section, contributing to the uncertainty affecting the results summarized in Figures 10 and S4, and Table 1. This uncertainty comes from the natural variability of the volcano dynamics as well as from the difficulty to reconstruct a robust record of major explosions over long periods. However, the temporal models of the occurrence probabilities of major explosions and paroxysms as a combined class, and only of the paroxysms, can provide additional insight on the scale parameter p (see Figure S7). In fact, the fraction between the peak hourly probabilities in the first weeks after an event considered in Figure 11, i.e., 0.05% and 0.013%, is ca. 25%, indicating that after a paroxysm, the parameter p can double with respect to a 12% "background" estimate. This is the reason why in Figure 11 we also considered a possible decoupling of the paroxysms occurrence probability from that of the major explosions plus paroxysms, under specific conditions.

Similarly, the statistics of the number of expected major explosions and paroxysms in the next 10 and 50 years, presented in Figure 12, can also provide estimates of the scale parameter p, if compared to the expected number of paroxysms in the same time intervals, according to the hourly probabilities in Figure S7. For example, after including the uncertain major explosions, the mean number of major explosions and paroxysms expected in the next 50 years is 117, and the mean number of paroxysms is 16, which would imply p = 14%, not far from 12%. However, it should be noted that, after excluding the uncertain major explosions in the next 50 years, the resulting p would increase to ca. 20%, confirming the significant uncertainty affecting this parameter, depending on the approach and data utilized to estimate it.

https://doi.org/10.5194/egusphere-2025-6540
Preprint. Discussion started: 12 January 2026

6 Conclusions

In this study, the first quantitative doubly stochastic probability maps of the areas potentially affected by ballistic fallout from major explosions and paroxysms, as well as from their combination, at Stromboli, have been presented. The hazard maps were based on a new database of simplified maps of the area affected by ballistics produced from the analysis of the rich information included in the historical and recent catalogs of the explosive activity of Stromboli, coming from all available scientific literature as well as from monitoring and field/observation reports, as described in Bevilacqua et al., (submitted). Moreover, the proposed hazard maps were based on the combination of three diverse and complementary models to statistically combine the distributions of directions and distances of ballistic fallout as estimated from the data. A key feature of the probabilistic hazard maps is also the quantitative description of the uncertainty associated with the reconstruction of the areas affected by ballistic fallout during past events.

In particular, the main findings of the study are:

1. Based on the frequency of available observations, ballistic dispersals from major explosions and paroxysms show distinct patterns which were illustrated by the so-called Model 1 (Figure 4a,b). For major explosions, ballistic dispersal is predominantly towards NE for contours below 35%, with a 2% probability up to about 400 m a.s.l., whereas contours over 35% are slightly asymmetric towards SE, i.e. the upper portion of Rina Grande. For paroxysms, all the contours are more extended towards NE and mostly towards WSW, with the 35% contours enclosing regions at 300 m a.s.l. in both directions, on the slopes above Ginostra and Stromboli villages, and about 20% probability of affecting the entire village of Ginostra.

2. To account for a likely under-sampling in the less accessible sectors of the island and for unobserved enhanced dispersal of ballistics in other directions due to potential variations in the morphology of craters and/or shallow part of conduits, Model 2 and Model 3 were introduced (Figure 4c,d,e,f). These two models dominate in distinct directions different from those of Model1, differing up to +/-15% in mean value. The maximum of the three Models in each location was then chosen to produce robust and, at the same time, conservative maps for major explosions and paroxysms, considered as separate categories (see Figures 6 and 7, respectively).

3. Given the substantial continuity of the main parameters characterizing the ballistic fallout for major explosions and paroxysms (Bevilacqua et al., submitted), and the present impossibility to predict with certainty the type of the next event, combined hazard maps for major explosions and paroxysms were also produced by assuming a relative proportion of the two categories as observed over the last few decades (Figures 8 and S3). For instance, assuming a relative proportion of events as in the period 2003-2023 (i.e., 12% or paroxysms over the total of paroxysms and major explosions), in the resulting mean map (Figure 8), the NE trails at 600 m are affected with ca. 25% probability, the viewpoints at 400 m a.s.l. on Labronzo trail and at 450 m on the Ginostra trail with ca. 8% and 7% probability, respectively. The viewpoint at 290 m on Labronzo trail and Ginostra Village are affected with ca. 5% and 3%

https://doi.org/10.5194/egusphere-2025-6540
Preprint. Discussion started: 12 January 2026

probability, respectively. The sea in front of Sciara del Fuoco is affected by ca. 2% probability up to 600 m from the shoreline whereas almost the entire Sciara is interested by probabilities above 5%.

4. The uncertainty associated with the reconstructed areas affected by ballistic fallout has an appreciable but overall limited effect. The 95th percentile contours are ca. 150 m larger than the 5th percentile equivalents, for major explosions, and up to 250 m larger, for paroxysms. Similarly, using the lower event ratio of major explosions and paroxysms as observed from 1970 to 2023 (7.3% instead of 12%) has also a limited effect. For instance, on the NE trails at ca. 600 m a.s.l. the probability decreases of ca. 5%, at the 400 m viewpoint on Labronzo trail the probability decreases of ca. 2%, and in Ginostra village of ca. 1.5%.

5. The product of the hourly probability of major explosions and paroxysms based on the occurrence model of Bevilacqua et al (2020a), and of the conditional hazard maps presented here, provides hourly hazard assessments of the areas affected by ballistic fallout (Figure 11). Hourly probabilities after 30 days of the last major explosion or paroxysm are about 0.05% whereas after 3 months without major explosions or paroxysms they decrease to about 0.025%. In addition, the hourly probability of the paroxysms shows a long-lasting increase, up to 0.013%, for over a year after every event of that type, which has significant implications in the resulting hazard maps, especially below 400 m a.s.l..

6. The combination of hourly probabilities and conditional hazard maps also produces probability maps of the areas affected by ballistic projectiles of at least one major explosion or paroxysm in the next 10 years (Figure 12). These maps also account for the occurrence of multiple major explosions and paroxysms. In particular, in the next 10 years Stromboli Village has 5% to 10% probability to be affected by ballistic fallout, and Ginostra 35% to 50%, respectively after excluding the uncertain major explosions from the temporal modeling or after including them.

The probabilistic hazard maps presented, either conditional on the occurrence of the event or over a specific time period, represent a first attempt to quantify the ballistic fallout hazard at Stromboli. Despite the several limitations of the approach followed as well as the still incomplete description of this activity, the maps are able to describe the main features of this phenomenon and associated hazard also including the quantification of some important sources of uncertainty. The maps represent a prerequisite to produce quantitative impact and risk assessments for the exposed individuals and buildings, once combined with vulnerability functions and exposure data (e.g. Baxter et al 2008; Neri et al 2008). Finally, the study highlights the importance of a close and continuous observation of the explosive activity of Stromboli aimed to quantify its dynamics and the dispersal of the associated products as well as of its simplified representation in order to produce quantitative hazard analyses.

https://doi.org/10.5194/egusphere-2025-6540
Preprint. Discussion started: 12 January 2026

Data availability

The full collection of simplified maps of major explosions and paroxysms is available in the companion study Bevilacqua et al. (submitted). The dataset of ASCII files of the presented probability maps is available at Bevilacqua et al. (2024b).

Author contributions

All authors gathered, cured, and discussed the historical data, their classification, and uncertainty quantification of the past ballistic dispersions. A.B. and A.N. conceived the main modeling ideas and scientific objectives. A.B. implemented the codes, performed the statistical analysis, and produced the graphs and maps. A.B. and A.N. prepared the first draft of the manuscript. All authors discussed the results, commented on the manuscript, provided critical feedback, and gave final approval for publication.

Competing interests

The contact author has declared that none of the authors has any competing interests.

Acknowledgements

This research has been supported by the INGV project “Rete Multiparametrica – Vulcani” and by “Piano di Potenziamento Stromboli EW-DPC, ex OCDPC n. 762/2021” and “Convenzione Attuativa per il potenziamento delle attività di servizio”, Task 4.1, in the framework of the “Accordo Quadro DPC-INGV 2022-2025”. The contribution and support of ideas of many colleagues participating in the above projects are acknowledged. The manuscript does not necessarily represent official views and policies of the Dipartimento della Protezione Civile.

https://doi.org/10.5194/egusphere-2025-6540
Preprint. Discussion started: 12 January 2026

References

Alatorre-Ibargüengoitia, M. A., Morales-Iglesias, H., Ramos-Hernández, S. G., Jon-Selvas, J., Jiménez-Aguilar, J. M. (2016), Hazard zoning for volcanic ballistic impacts at El Chichón Volcano (Mexico). *Nat Hazards* 81, doi:10.1007/s11069-016-2152-0.

Andronico, D., and Pistolesi, M. (2010). The November 2009 paroxysmal explosions at Stromboli. *J Volcanol Geoth Res* 196(1-2), 120-125, doi: 10.1016/j.jvolgeores.2010.06.005.

Andronico, D., Del Bello, E., D'Oriano, C., Landi, P., Pardini, F., Scarlato, P., de' Michieli Vitturi, M., Taddeucci, J., Cristaldi, A., Ciancitto, F., Pennacchia, F., Ricci, T., and Valentini, F. (2021). Uncovering the eruptive patterns of the 2019 double paroxysm eruption crisis of Stromboli volcano. *Nat Comm* 12(1), 4213, doi: 10.1038/s41467-021-24420-1.

Aravena, A., Bevilacqua, A., Neri, A., Gabellini, P., Ferrés, D., Escobar, D., Aiuppa, A., Cioni, R. (2023) Scenario-based probabilistic hazard assessment for explosive events at the San Salvador volcanic complex, El Salvador, *J Volcanol Geoth Res* 438, 107809.

Barberi, F., Rosi, M., Sodi, A. (1993), Volcanic hazard assessment at Stromboli based on review of historical data, *Acta Vulc*, 3, 173–187.

Baxter, P.J. and A. Gresham, (1997). Deaths and injuries in the eruption of Galeras Volcano, Colombia, J Volcanol Geoth Res 77, 325-338. doi: 10.1016/S0377-0273(96)00103-5.

Baxter P.J., W. Aspinall, A. Neri, G. Zuccaro, R.S.J. Spence, R. Cioni, G. Woo (2008). Emergency planning and mitigation at Vesuvius: A new evidence-based approach, *J Volcanol Geoth Res* 178, 3, 454-473, doi: 10.1016/j.jvolgeores.2008.08.015 (1).

Bebbington, M. S. (2013). Assessing spatio-temporal eruption forecast in a monogenetic volcanic field. *J Volcanol Geoth Res* 252, 14–28.

Bernard, B. (2018), Rapid hazard assessment of volcanic ballistic projectiles using long-exposure photographs: insights from the 2010 eruptions at Tungurahua volcano, Ecuador. *Volcanica* 1(1): 49 – 61. doi: 10.30909/vol.01.01.4961.

Bertagnini, A., Coltelli, M., Landi, P., Pompilio, M., and Rosi, M. (1999). Violent explosions yield new insights into dynamics of Stromboli volcano. *Eos, Trans Am Geoph Union* 80(52), 633-636, doi: 10.1029/99EO00415.

Bertagnini, A., Metrich, N., Francalanci, L., Landi, P., Tommasini, S., Conticelli, S. (2008), Volcanology and magma geochemistry of the present-day activity: constraints on the feeding system. In: Calvari S, Inguaggiato S, Puglisi G, Ripepe M, Rosi M (eds) Learning from Stromboli. American Geophysical Union, *Geophys Mono* 182, Washington, DC, pp 19–38.

Bertagnini, A., Di Roberto, A., Pompilio, M. (2011), Paroxysmal activity at Stromboli: lessons from the past. *Bull Volc* 73 doi: 10.1007/s00445-011-0470-3.

Bertin, D. (2017), 3-D ballistic transport of ellipsoidal volcanic projectiles considering horizontal wind field and variable shape-dependent drag coefficients, *J Geophys Res - Solid Earth* 122, 1126–1151, doi: 10.1002/2016JB013320.

Bevilacqua, A., R. Isaia, A. Neri, S. Vitale, W.P. Aspinall, M. Bisson, F. Flandoli, P. J. Baxter, A. Bertagnini, T. Esposti Ongaro, E. Iannuzzi, M. Pistolesi, and M. Rosi (2015), Quantifying volcanic hazard at Campi Flegrei *caldera* (Italy) with uncertainty assessment: I. Vent opening maps, *J Geophys Res – Solid Earth* 120, 2309-2329, doi: 10.1002/2014JB011775.

Bevilacqua, A. (2016), Doubly stochastic models for volcanic hazard assessment at Campi Flegrei caldera, Theses, 21, Edizioni della Normale, Birkhäuser/Springer, 227p, Pisa, doi: 10.1007/978-88-7642-577-6, ISBN 978-88-7642-577-6.

https://doi.org/10.5194/egusphere-2025-6540
Preprint. Discussion started: 12 January 2026

Bevilacqua, A., Flandoli, F., Neri, A., Isaia, R., & Vitale, S. (2016), Temporal models for the episodic volcanism of Campi Flegrei caldera (Italy) with uncertainty quantification. *J Geophys Res: Solid Earth*, 121, 7821–7845. doi: 10.1002/2016JB013171.

Bevilacqua, A., A. Neri, M. Bisson, T. Esposti Ongaro, F. Flandoli, R. Isaia, M. Rosi, S. Vitale (2017), Effects of vent location, event scale and time forecasts on pyroclastic density currents hazard maps at Campi Flegrei caldera, (Italy), *Front in Earth Sci* 5, 72, 1-16, doi: 10.3389/feart.2017.00072.

Bevilacqua, A., Bursik, M., Patra, A., Pitman, E. B., Yang, Q., Sangani, R., & Kobs-Nawotniak, S. (2018), Late Quaternary eruption record and probability of future volcanic eruptions in the Long Valley volcanic region (CA, USA). *J Geophys Res: Solid Earth* 123, 5466–5494. doi: 10.1029/2018JB015644.

Bevilacqua A., A. Bertagnini, M. Pompilio, P. Landi, P. Del Carlo, A. Di Roberto, W. Aspinall, and A. Neri, (2020a). Major explosions and paroxysms at Stromboli (Italy): a new historical catalog and temporal models of occurrence with uncertainty quantification. *Sci Rep*, 10, 17357. doi: 10.1038/s41598-020-74301-8.

Bevilacqua A., Bertagnini A., Pompilio, M., Landi, P., Del Carlo, P., D Roberto, A., Piccione, C., Neri, A. (2020b), Historical catalog of major explosions and paroxysms at Stromboli (Italy) [Dataset]. *INGV Ufficio Dati*, doi: 10.13127/STROMBOLI/STRCATALOG.

Bevilacqua A., Bertagnini A., Pompilio, M., Landi, P., Del Carlo, P., D Roberto, A., Piccione, C., Falsaperla, S., Spampinato, S., Neri, A. (2023), Catalog of major explosions and paroxysms at Stromboli volcano (Italy) from 1970 to 2023 [Dataset]. *INGV Ufficio Dati*, doi: 10.13127/STROMBOLI/STRCATALOG2.

Bevilacqua, A., Landi, P., Del Carlo, P., Neri, A., Pompilio, M. (submitted), Ballistic projectile hazard of major explosions and paroxysms at Stromboli (Italy) with uncertainty quantification: 1. Mapping method and data analysis, doi: 10.5194/egusphere-2025-6539.

Bevilacqua, A., Nannipieri, L., Favalli, M., Fornaciai, A. (2024a), UAS-based mapping of the July 3, 2019, ballistics density distribution on the W flank of Stromboli with uncertainty quantification. *Bull Volcanol* 86, 48, doi: 10.1007/s00445-024-01741-9.

Bevilacqua, A., Neri, A., Landi, P., Del Carlo, P., Pompilio, M. (2024b). Database of probability maps supporting: "Quantifying ballistic projectile hazard of major explosions and paroxysms at Stromboli (Italy) with uncertainty assessment: 2. probability maps" [Data set]. Zenodo. doi: 10.5281/zenodo.14268921.

Biass, S., Falcone, J.L, Bonadonna, C., Di Traglia, F., Pistolesi, M., Rosi, M., Lestuzzi, P. (2016) Great Balls of Fire: A probabilistic approach to quantify the hazard related to ballistics — A case study at La Fossa volcano, Vulcano Island, Italy, *J Volcanol Geoth Res* 325, 1-14, do: 10.1016/j.jvolgeores.2016.06.006.

Bisson, M., Spinetti, C., Gianardi, R., Strehlow, K., De Beni, E., Landi, P. (2023), High-resolution mapping and dispersion analyses of volcanic ballistics emitted during the 3rd July 2019 paroxysm at Stromboli. *Sci Rep* 13:13465.

Breard, E.C.P., Lube, G., Cronin, S.J., Fitzgerald, R., Kennedy, B., Scheu, B., Montanaro, C., White, J.D.L., Tost, M., Procter, J.N., Moebis, A. (2014), Using the spatial distribution and lithology of ballistic blocks to interpret eruption sequence and dynamics: August 6 2012 Upper Te Maari eruption, New Zealand, *J Volcanol Geoth Res* 276, 383-376.

Brown, S. K., Jenkins, S. F., Stephen, R., Sparks, J., Odbert, H., Auker, M. R. (2017), Volcanic fatalities database: analysis of volcanic threat with distance and victim classification. J Appl Volcanol 6, 15, doi: 10.1186/s13617-017-0067-4.

https://doi.org/10.5194/egusphere-2025-6540
Preprint. Discussion started: 12 January 2026

Capaldi, G., Guerra, I., Lo Bascio, A. et al. Stromboli and its 1975 eruption. Bull Volcanol 41, 259-285 (1978). https://doi.org/10.1007/BF02597227.

Carcano, S., Bonaventura, L., Esposti Ongaro, T., Neri, A. (2013). A semi-implicit, second-order-accurate numerical model for multiphase underexpanded volcanic jets. *Geosci Model Dev* 6:1905–1924, doi: 10.5194/gmd-6-1905-2013.

Coltelli, M., Del Carlo, P., and Pompilio, M. (2000). Vulcano and Stromboli, 1. Eruptive History (Stromboli), *Acta Vulc* 12, 93-95.

Davies, P., (1993). A guide to the evaluation of condensed phase explosions, J Hazardous Mat 33, 1 - 33. doi: 10.1016/0304-3894(93)85061-I.

Deligne, N.I., Jolly, G.E., Taig, T. et al. Evaluating life-safety risk for fieldwork on active volcanoes: the volcano life risk estimator (VoLREst), a volcano observatory's decision-support tool. J Appl. Volcanol. 7, 7 (2018). doi: 10.1186/s13617-018-0076-y

de' Michieli Vitturi, M., A. Neri, T. Esposti Ongaro, S. Lo Savio, and E. Boschi (2010), Lagrangian modeling of large volcanic particles: Application to Vulcanian explosions, *J Geophys Res* 115, B08206, doi: 10.1029/2009JB007111.

Esposti Ongaro, T., Neri, A., Menconi, G., de'Michieli Vitturi, M., Marianelli, P., Cavazzoni, C., Erbacci, G., Baxter, P.J. (2008) Transient 3D numerical simulations of column collapse and pyroclastic density current scenarios at Vesuvius. *J Volcanol Geotherm Res* 178:378-396, doi: 10.1016/j.jvolgeores.2008.06.036.

Fitzgerald, R. H., Tsunematsu, K., Kennedy, B. M., Breard, E. C. P., Lube, G., Wilson, T. M., Jolly, A. D., Pawson, J., Rosenberg, M. D., Cronin, S. J. (2014), The application of a calibrated 3D ballistic trajectory model to ballistic hazard assessments at Upper TeMaari, Tongariro. *J Volcanol Geoth Res* 286, 248–262.

Fitzgerald, R. H., Kennedy, B. M., Wilson, T. M., Leonard, G. S., Tsunematsu, K., Keys, H. (2018), The communication and risk management of volcanic ballistic hazards. In: *Observing the Volcano World, Volcano Crisis Communication*. Fearnley, C. J., Bird, D. K., Haynes, K., McGuire, W. J., Jolly, G. (Eds), Springer Open. *Advs in Volcanology*, 121–147.

Giordano, G., and De Astis, G. (2021). The summer 2019 basaltic Vulcanian eruptions (paroxysms) of Stromboli. *Bull Volcanol* 83, 1-27, doi: 10.1007/s00445-020-01423-2.

Graettinger, A.H. , Valentine, G.A., Sonder, I., (2015), Circum-crater variability of deposits from discrete, laterally and vertically migrating volcanic explosions: Experimental evidence and field implications, *J Volcanol Geoth Res* 308, 61-69, doi: 10.1016/j.jvolgeores.2015.10.019.

Guardo, R., Bilotta, G., Ganci, G., Zuccarello, F., Andronico, D., Cappello, A. (2024), Modeling Fire Hazards Induced by Volcanic Eruptions: The Case of Stromboli (Italy). *Fire* 7, 70. doi: 10.3390/fire7030070.

Gurioli, L., Harris, A. J. L., Colo, L., Bernard, J., Favalli, M., Ripepe, M., Andronico, D. (2013), Classification, landing distribution, and associated flight parameters for a bomb field emplaced during a single major explosion at Stromboli, Italy. *Geology* 41(5), 559–562.Iacono, F., Bisson, M., Spinetti, C., and Kwasnitschka, T. (2025). Wildfires Induced by Volcanic Activity at Stromboli Island during the 2019 Summer through Satellite and Drone Data. Remote Sens Earth Syst Sci 8, 733–752. doi: 10.1007/s41976-025-00215-6.

Jolly, G.E., Keys, H.J.R., Procter, J.N., Deligne, N.I. (2014) Overview of the co-ordinated risk-based approach to science and management response and recovery for the 2012 eruptions of Tongariro volcano, New Zealand. JVGR 286, 184-207.

https://doi.org/10.5194/egusphere-2025-6540
Preprint. Discussion started: 12 January 2026

Konstantinou, K. I. (2015), Maximum horizontal range of volcanic ballistic projectiles ejected during explosive eruptions at Santorini caldera. J. *Volcanol. Geoth. Res.* 301, 107–115.

Maeno, F., Nakada, S., Nagai, M., Kozono, T. (2013), Ballistic ejecta and eruption condition of the vulcanian explosion of Shinmoedake volcano, Kyushu, Japan on 1 February, 2011, *Earth Planets Space* 65, 609–621.

Marzocchi, W.,&Bebbington, M. S. (2012). Probabilistic eruption forecasting at shortandlong time scales. *Bull Volcanol* 74, 1777–1805.

Massaro, S., Rossi, E., Sandri, L., Bonadonna, C., Selva, J., Moretti, R., Komorowski, J.C. (2022), Assessing hazard and potential impact associated with volcanic ballistic projectiles: The example of La Soufrière de Guadeloupe volcano (Lesser Antilles), *J Volcanol Geoth Res* 423, 107473.

Nappi, G. (1977). Rischio vulcanico e sorveglianza nei Campi Flegrei e nell'isola di Stromboli. *Boll Soc Geo Ita* 98, 141-156.

Neri, A., A. Bevilacqua, T. Esposti Ongaro, R. Isaia, W.P. Aspinall, M. Bisson, F. Flandoli, P. J. Baxter, A. Bertagnini, E. Iannuzzi, S. Orsucci, M. Pistolesi, M. Rosi, and S. Vitale (2015), Quantifying volcanic hazard at Campi Flegrei caldera (Italy) with uncertainty assessment: II. Pyroclastic density current invasion maps, *J Geophys Res – Solid Earth* 120, 2330-2349, doi: 10.1002/2014JB011776.

Neri A., W.P. Aspinall, R. Cioni, A. Bertagnini, P.J. Baxter, G. Zuccaro, D. Andronico, S. Barsotti, P.D. Cole, T. Esposti Ongaro, T.K. Hincks, G. Macedonio, P. Papale, M. Rosi, R. Santacroce, G. Woo (2008). Developing an Event Tree for Probabilistic Hazard and Risk Assessment at Vesuvius, *J Volcanol Geoth Res* 178, 3, 397-415, doi: 10.1016/j.jvolgeores.2008.05.014.

Ogden, D.E.,Wohletz, K.H., Brodski, E.E., Glatzmaier, G.A., (2007). Numerical simulation of volcanic jets: importance of vent overpressure. *J Geophys Res* 113, B02204, doi:10.1029/2007JB005133.

Pistolesi, M., D. Delle Donne, L. Pioli, M. Rosi, and M. Ripepe (2011), The 15 March 2007 explosive crisis at Stromboli volcano, Italy: Assessing physical parameters through a multidisciplinary approach, *J Geophys Res* 116, B12206, doi: 10.1029/2011JB008527.

Pompilio, M., Bertagnini, A., Di Roberto, A. (2010) Present-day activity of Stromboli: eruptive history and eruptive styles, *Acta Vulc* 22 (1-2), 29-34.

Re, G., Di Roberto, A., Del Carlo, P., Pompilio, M. (2025). Evolution of the eruptive activity at Stromboli (Aeolian Islands - Italy) during the last 4 millennia. A tephrostratigraphic investigation on the early-phase of Recent Stromboli Eruptive Epoch. J Volcanol Geotherm Res, 462, 108308, https://doi.org/10.1016/j.jvolgeores.2025.108308.

Rittmann, A. (1931): Der Ausbruch des Stromboli am 11 September 1930. Zeits Vulkanol 14, 47-77.

Rosi, M., Bertagnini, A., Harris, A. J. L., Pioli, L., Pistolesi, M., and Ripepe, M. (2006). A case history of paroxysmal explosion at Stromboli: timing and dynamics of the April 5, 2003 event. *Earth Planet Sci Lett* 243(3-4), 594-606, doi: 10.1016/j.epsl.2006.01.035.

Rosi, M., Pistolesi, M., Bertagnini, A., Landi, P., Pompilio, M., Di Roberto, R. (2013), Stromboli volcano, Aeolian Islands (Italy): present eruptive activity and hazards. In: Lucchi, F., Peccerillo, A., Keller, J., Tranne, C. A., Rossi, P. L. (eds) 2013. *The Aeolian Islands Volcanoes*. *Geological Society, London, Memoirs* 37, 473–490. doi: 10.1144/M37.14.

Rosi, M., Di Traglia, F., Pistolesi, M. et al. (2018), Dynamics of shallow hydrothermal eruptions: new insights from Vulcano's Breccia di Commenda eruption. *Bull Volcanol* 80, 83, doi: 10.1007/s00445-018-1252-y.

https://doi.org/10.5194/egusphere-2025-6540
Preprint. Discussion started: 12 January 2026

Rutarindwa, R., Spiller, E. T., Bevilacqua, A., Bursik, M. I., & Patra, A. K. (2019). Dynamic probabilistic hazard mapping in the Long Valley Volcanic Region CA: Integrating vent opening maps and statistical surrogates of physical models of pyroclastic density currents. *J Geophys Res : Solid Earth* 124. doi: 10.1029/2019JB017352.

Schmid, M., Kueppers, U., Ricci, T., Civico, R., Cigala, V., Fee, D., Gestrich, J. E., Iezzi, A. M., Cimarelli, C., Vossen, C. E. J., Buzard, R. M., Ripepe, M., Lacanna, G. and Dingwell, D. B. (2025) "The morphological response to the 13 May 2022 major explosive event at Stromboli volcano, Italy, characterised by high-resolution UAS surveys", Volcanica, 8(2), pp. 387–397. doi: 10.30909/vol/crjj4989.

Sparks, R. S. J., & Aspinall, W. A. (2004). Volcanic activity: Frontiers and challenges in forecasting, prediction and risk assessment, in: The state of the planet, Frontiers and challenges in geophysics, *Geophys Mono 150*, IUGG, 19, 359–373.

Taddeucci, J., G. A. Valentine, I. Sonder, J. D. L. White, P. S. Ross, and P. Scarlato (2013), The effect of pre-existing craters on the initial development of explosive volcanic eruptions: An experimental investigation, *Geophys Res Lett* 40, 507–510, doi: 10.1002/grl.50176.

Taddeucci, J., Alatorre-Ibargüengoitia, M.A., Cruz-Vàzquez, O., Del Bello, E., Scarlato, P., Ricci, T. (2017), In-flight dynamics of volcanic ballistic projectiles. *Rev of Geophys* 55 675-718. doi: 10.1002/2017RG000564.

TNO, (1992). Methods for the determination of possible damage to people and objects resulting from release of hazardous materials. Nederlandse organisatie voor toegepast-natuurwetenschappelijk onderzoek (TNO), 337pp, Committee for the Prevention of Disasters, The Hague, ISBN 90-5307-052-4.Tsunematsu, K., Chopard, B., Falcone, J.L., Bonadonna, C. (2015), A numerical model of ballistic transport with collisions in a volcanic setting, *Comp & Geosci* 63, 62-69, doi: 10.1016/j.cageo.2013.10.016.

Turchi, A., F. Di Traglia, T. Luti, D. Olori, I. Zetti and R. Fanti (2020). Environmental aftermath of the 2019 Stromboli eruption, *Remote Sens* 12(6), 994.

Valentine, G. A., J. D. L. White, P.-S. Ross, J. Amin, J. Taddeucci, I. Sonder, and P. J. Johnson (2012), Experimental craters formed by single and multiple buried explosions and implications for volcanic craters with emphasis on maars, *Geophys Res Lett* 39, L20301, doi: 10.1029/2012GL053716.

Vanderkluysen, L., Harris, A.J.L., Kelfoun, K. et al. (2012) Bombs behaving badly: unexpected trajectories and cooling of volcanic projectiles. *Bull Volcanol* 74, 1849–1858. doi: 10.1007/s00445-012-0635-8.

Williams, G.T., Kennedy, B.M., Wilson, T.M., Fitzgerald, R.H., Tsunematsu, K., Teissier, A. (2017), Buildings vs. ballistics: Quantifying the vulnerability of buildings tovolcanic ballistic impacts using field studies and pneumatic cannon experiments. *J Volcanol Geoth Res* 343, 171-180.

Wilson, L. (1972), Explosive Volcanic Eruptions-II The Atmospheric Trajectories of Pyroclasts, *Geophys J Internat* 30 (4), 381–392, doi: 10.1111/j.1365-46X.1972.tb05822.x.